EPSC2017

SB4 abstracts

EPSC Abstracts
Vol. 11, EPSC2017-14, 2017
European Planetary Science Congress 2017

Asteroids as tracers of solar system formation: Probing the interior of primordial main belt asteroids

P. Vernazza (1), F. Marchis (2), B. Carry (3), M. Marsset (4), J. Hanus (5), T. Santana-Ros (6), M. Birlan (7), C. Dumas (8), M. Viikinkoski (9), M. Kaasalainen (9), B. Yang (10), J. Durech (5), L. Jorda (1), P. Lamy (1), A. Vigan (1), T. Fusco (1), T. Michalowski (6), A. Marciniak (6), P. Bartczak (6), M. Pajuelo (7), P. Michel (3), P. Tanga (3), J. Berthier (7), F. Vachier (7), J. Castillo-Rogez (11), O. Witasse (12), F.Cipriani (12), S. Lindsay (13), E. Jehin (14).
(1) Laboratoire d'Astrophysique de Marseille, France, (pierre.vernazza@lam.fr / Phone: +33-4-91055911) (2) Seti institute, USA, (3) OCA, France, (4) Queen's University of Belfast, UK, (5) Charles University in Prague, CZ, (6) Astronomical Observatory Institute, Faculty of Physics, Adam Mickiewicz University, PL, (7) IMCCE, FR, (8) TMT, USA, (9) TUT, Finland, (10) ESO, CL, (11) JPL, USA, (12) ESTEC, NL, (13) Univ of Tennessee, USA, (14) Institut d'Astrophysique de l'Université de Liège , BE

Abstract

Asteroids in our solar system are metallic, rocky and/or icy objects, ranging in size from a few meters to a few hundreds of kilometers. Whereas we now possess constraints for the surface composition of most D>100 km primordial main-belt asteroids, little is known regarding their internal structure. Yet, this is a fundamental property whose characteristics result directly from (a) their formation location, (b) their time of formation, and (c) their collisional history. Characterizing the internal structure of the main compositional classes of asteroids would therefore allow us to address entirely new questions regarding the earliest stages of planetesimal formation and their subsequent collisional and dynamical evolution.

To achieve this goal, we will - *via an ESO Large Program (LP) that was awarded 152h on VLT/SPHERE (the observations will be spread over 4 semesters from April 1st, 2017 till March 30, 2019 in service mode)* - carry out a survey of a substantial fraction of all D≥100 km main-belt asteroids for the four major compositional classes (8 to 10 objects per class for the following groups of classes: S, Ch/Cgh, B/C and P/D; objects belonging to these classes represent more than 90% of the mass of the asteroid belt, see DeMeo & Carry 2013) at high angular-resolution with VLT/SPHERE throughout their rotation in order to derive their volume (via their 3-D shape; see Fig. 1), which combined with already existing mass estimates will allow us to determine their bulk density. The high-resolution 3-D shapes will also allow us to detect craters larger than ~30 km and thus use their morphology (crater diameter and depth) to characterize the density of the outer shell. The knowledge of both their bulk density and the density of their outer shell will allow us to characterize their internal structure. This information, in turn, will allow us to determine: (a) the nature of the initial building blocks (rock only, or a mixture of ice and rock) and (b) which compositional classes experienced differentiation. These constraints will serve as direct inputs to thermal evolution models and allow us determine the time of formation as well as the formation location (inward or outward of the snowline) of the main compositional classes.

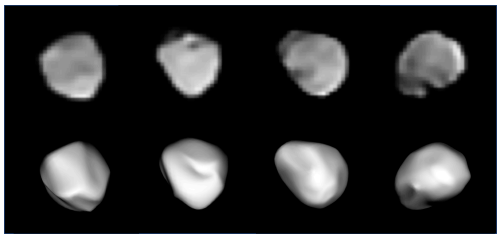

Figure 1 (from Marsset et al. 2017, submitted): **Expected output from our survey: high-resolution shapes, accurate densities and reconnaissance of the largest craters for ~40 D>100km main belt asteroids.** Here, SPHERE images of (6) Hebe acquired throughout its rotation and used for reconstruction (top) and corresponding model views (bottom).

Importantly, our survey will provide key constraints to solar system formation models such as the Nice and Grand Tack ones (e.g., Morbidelli et al. 2005, Levison et al. 2009, Walsh et al. 2011). These models propose that today's asteroid belt may not only hosts objects that formed in situ (hence, rocky-rich),

typically between 2.2 and 3.3 AU (probably the case for the so-called S-types), but also a substantial fraction of bodies (≥50%) that were formed in the giant planet region and beyond (hence, water/ice-rich). Our density estimates will allow testing this hypothesis as we should find a substantial fraction of bodies with densities compatible with those of comets and trans-Neptunian objects (density≤1.2 g/cm^3).

Here, we will present the very first results of our survey that started April 1st, 2017.

EPSC Abstracts
Vol. 11, EPSC2017-50, 2017
European Planetary Science Congress 2017

Rotation-induced YORP break-up of small bodies to produce post-main-sequence debris

Dimitri Veras (1), Seth A. Jacobson (2,3), Boris T. Gänsicke (1)
(1) Department of Physics, University of Warwick, Coventry CV4 7AL, UK
(2) Laboratoire Lagrange, Observatoire de la Coˆte d'Azur, Boulevard de l'Observatoire, F-06304 Nice Cedex 4, France
(3) Bayerisches Geoinstitut, Universtät Bayreuth, D-95440 Bayreuth, Germany
(d.veras@warwick.ac.uk)
Based on MNRAS (2014), 445, 2794-2799

Abstract

We hypothesize that the in situ break-up of small bodies such as asteroids spun to fission during the giant branch phases of stellar evolution provides an important contribution to the debris orbiting and ultimately polluting white dwarfs. The YORP (Yarkovsky–O'Keefe–Radviesvki–Paddock) effect, which arises from radiation pressure, accelerates the spin rate of asymmetric asteroids, which can eventually shear themselves apart. This pressure is maintained and enhanced around dying stars because the outward push of an asteroid due to stellar mass loss is insignificant compared to the resulting stellar luminosity increase. Consequently, giant star radiation will destroy nearly all bodies with radii in the range 100 m–10 km that survive their parent star's main-sequence lifetime within a distance of about 7 au; smaller bodies are spun apart to their strongest, competent components. This estimate is conservative and would increase for highly asymmetric shapes or incorporation of the inward drag due to giant star stellar wind. The resulting debris field, which could extend to thousands of au, may be perturbed by remnant planetary systems to reproduce the observed dusty and gaseous discs which accompany polluted white dwarfs.

1. Introduction

Asteroids likely represent the primary source of the metal pollution in white dwarf atmospheres. The YORP effect on asteroids has been well-established in the solar system [3], but rarely addressed in other planetary systems. [2] proposes that many asteroids will not survive the giant branch stages of stellar evolution intact due to radiation-induced rotational fission. Consequently, the reservoir of material available to form discs around white dwarfs is composed of smaller fragments than what was previously assumed.

The YORP effect is the rotational acceleration of a body due to the anisotropic absorption and radiation of light. The effect was first proposed in the context of absorbing stellar UV and visible light and the emittance of thermal radiation due to the local heating of the body [1], although the role of conducted heat is now considered possibly as important. Observationally measured rotational acceleration of a number of asteroids has matched predictions from the YORP theory.

The Sun's luminosity will increase by a factor of thousands after it leaves the main sequence, significantly enhancing the YORP effect. Other stars more massive than the Sun will increase their luminosity by greater factors.

2. Figures

In [2], we perform simulations that showcase the extent of rotational disruption when the parent star leaves the main sequence. We assume, conservatively, that all asteroids begin evolving during giant branch evolution without any spin and that the asteroid shape does not change. The eccentricity of the asteroid remains constant, as adiabatic mass-loss predicts. Both the luminosity of the star and the semimajor axis of the asteroid are varied; the latter is varied adiabatically and so is independent of initial orbital orientation. We model the evolution of stars with main-sequence progenitor masses of 1–5 $M_{\odot}$, as these likely represent the range of progenitor masses which have yielded the vast majority of currently observed white dwarfs.

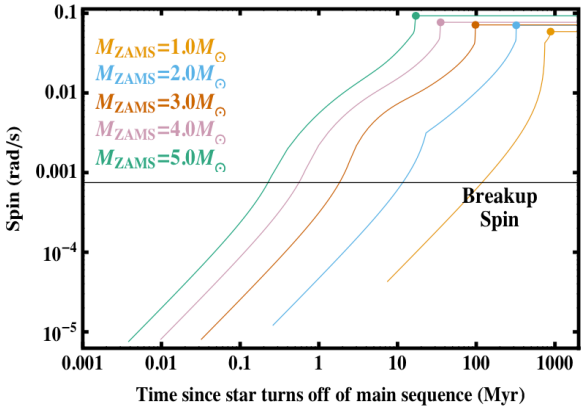

Figure 1: A demonstration of why asteroid belts will be destroyed during giant branch evolution. This plot features the spin-up of objects with radii of R = 1 km, an initial semimajor axis of 7.0 au and an eccentricity of zero. The objects have typical asteroid densities of ρ = 2 g cm^{-3} and a 1% degree of asymmetry. The horizontal black line represents the critical spin value at which an asteroid will tear itself apart. All objects are assumed to begin life on the giant branch with no spin, and the curves are drawn from the beginning of the red giant branch phases. Dots indicate when the stars become white dwarfs. The stars are all assumed to initially harbour Solar metallicity.

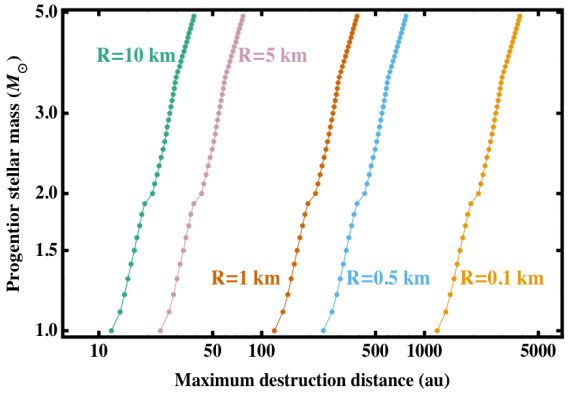

Figure 2: The maximum (final) distance, or semimajor axis, at which asteroids with forever circular orbits, a radius *R*, density of 2 g cm^{-3} and asymmetry parameter 0.01 can be destroyed by YORP. Each dot represents the result of an integration initilized with the highest initial semi-major axis for which destruction occurs.

3. Conclusions

We have identified a potentially significant source of debris in post-main-sequence planetary systems: the remains of asymmetric asteroids which have spun up beyond their breaking points due to stellar radiation during the giant branch stages of stellar evolution. Typical asymmetric asteroids with radii between about 100 m and 10 km that reside within about 7 au of the star during the main sequence will be destroyed, leaving a debris field orbiting white dwarfs at distances which can range from a few tens to a few thousands of au. Objects larger than 10 km in size will be largely unaffected by YORP. The majority of the asteroidal-based mass would be contained in these large objects, such as analogues of Ceres and Vesta. The debris from rotational break-up may provide a reservoir for white dwarf disc creation and ultimately atmospheric pollution. White dwarf luminosity itself is too low to destroy asteroids in time-scales within Gyr unless the asteroids are already spinning near the break-up speed.

Acknowledgements

DV and BTG have received funding from the European Research Council under the European Union's Seventh Framework Programme (FP/2007-2013)/ERC Grant Agreement no. 320964 (WDTracer).

References

[1] Rubincam, D.P.: Radiative Spin-up and Spin-down of Small Asteroids, Icarus, Vol. 148, 2-11, 2000.

[2] Veras, D., Jacobson, S.A., Gänsicke, B.T.: Post-main-sequence debris from rotation-induced YORP break-up of small bodies, MNRAS, Vol. 445, 2794-2799, 2014.

[3] Vokrouhlicky, D., Bottke, W.F., Chesley, S.R., Scheeres, D.J., Statler, T.S.: The Yarkovsky and YORP Effects. In Asteroids IV. Eds. Patrick Michel, Francesca E. DeMeo and William F. Bottke Jr.; The University of Arizona Press, 2015.

EPSC Abstracts
Vol. 11, EPSC2017-105, 2017
European Planetary Science Congress 2017

Asteroid 2014J025 confirms characteristic convexo-concave with a deep rift shape of many small cosmic bodies

G. Kochemasov, IGEM of Russian Academy of Sciences, 35 Staromonetny, 119017, Moscow, RF, kochem.36@mail.ru

The wave warping of celestial bodies due to their movement in non-circular keplerian orbits with periodically changing accelerations is especially notable in shapes of small bodies (asteroids, comet cores, satellites).They are often bent by the fundamental wave 1 and acquire shapes of “dumb-bells’, “bean”, “peanut” and often are disintegrated into two or several peaces moving in an original or slightly different orbits. The disintegration is provoked by nearing deep fissures of the convex hemisphere with diminishing distance of the concave one to the fissures. Thus a “neck” develops (Fig. 1- 9).

The classical planetology considers impacts as a main source of energy reworking celestial bodies. However a region or regions of impacting objects affecting all planetary bodies everywhere in the Solar system is poorly understood. But now planetologists have several tens of images of full discs of these bodies. Distribution patterns of “impact traces” – craters in many of them are surprisingly regular. They show alignments, regular grids not related to random hits expected from impacts but rather require more regular and ubiquitous structuring force.

It was shown earlier [1-5] that such regular patterns appear due to warping action of inertia-gravity waves affecting all bodies moving in keplerian elliptical orbits. Periodically changing accelerations of celestial bodies cause their wave warping having in rotating bodies (but all bodies rotate!) four ortho- and diagonal directions. An interference of 4 directions of standing waves brings about a regular net of uprising, subsiding and neutral tectonic blocks. Naturally polygonal in details they appear as rings in cosmic images. This is one of reasons why they are often confused with round impact craters and essentially disfigure their statistics.

A fundamental nature of the wave woven nets of evenly sized round “craters” (granules) is dependence of their sizes on orbital frequencies of bodies. The lower frequency the larger sizes, the higher frequency the smaller granule sizes.

The correspondence between orbital frequencies and tectonic granulations proving the structuring role of orbital energy was earlier noted in comparative planetology of the terrestrial planets. The row of Mercury, Venus, Earth, Mars, asteroids with decreasing orbital frequencies is remarkable by increasing relative sizes of tectonic granules, relief ranges, iron content in lowland basalts and decreasing atmospheric masses from Venus to Mars.

In this spectacular row the position of asteroids is especially remarkable. The strongest amplitude fundamental wave1 embraces an asteroid body making it strongly bent. Its extended convex hemisphere is deeply cracked and the concave one from the opposite site approaches the deepest fissures (Fig. 4). As a result the body tends to disintegrates and two or several pieces move as binaries, polycomponent asteroids, and asteroids with satellites. Two-lobed dumb-bells shapes often are observed also among comet cores and small satellites (Fig. 5, 6, 9). Examples of various stages of this destruction are asteroids Eros, Toutatis, Braille, Castalia, Hector, and recently observed P/2013R3 that shows enormous volumes of gas-dust clouds accompanying the process. The orbiting clouds in the past may have been a media for gravity separation of M-, S-, and C-asteroids. The denser M-asteroids enrich the inner main asteroid belt and the less dense S-asteroids the outer part of the belt fragments.

Several images of small cosmic bodies presented here (fig. 1 to 9) show characteristic bends producing thin parts – “necks” in the middle parts of the bodies and thickenings in their ends (two-lobed forms). Thus, necks are a result of breaking of a whole body [3, 5]. In some rare cases an assemblage of alien fragments also is possible [6]. In future, cosmic robots placed at “neck” regions of various small bodies should resolve this question by measuring composition and structure of small pieces around. If they are uniform, they are fragments of one body, if not, two different bodies possibly are assembled. Asteroid 2014J025 shows typical forms of a small body deformed (warped, bent and deeply cut) by the inertia-gravity waves (wave1 and shorter ones) due to moving in an

elliptical orbit. External orbital energy is a main energetic source structuring cosmic bodies [1-5].

References: [1] Kochemasov, G.G. Tectonic dichotomy, sectoring and granulation of Earth and other celestial bodies // Proceedings of the International Symposium on New Concepts in Global Tectonics, "NCGT-98 TSUKUBA", Geological Survey of Japan, Tsukuba, Nov 20-23, 1998, p. 144-147.**[2]** Kochemasov, G.G. Theorems of wave planetary tectonics // Geophys. Res. Abstr. 1999. V.1, №3, p. 700. **[3]** Kochemasov G.G. "Diamond" and "dumb-bells"-like shapes of celestial bodies induced by inertia-gravity waves // The 30th Vernadsky-Brown microsymposium on comparative planetology, Abstracts, Moscow, GEOKHI, 1999, 49-50.

[4] Kochemasov G.G. Celestial bodies: relation between ubiquitous tectonic dichotomy and universal rotation //NCGT Journal, v. 3, # 2, June 2015, 155-157. **[5]** Kochemasov G.G. Characteristic "necks" of small cosmic bodies: formation in process of breaking or smooth impact (sticking together) of two fragments // 48th LPSC (2017), Abstract # 1092; **[6]** Ksanfomality L., Zelenyi L. Does regional surface morphology of comets 67P/CG and 1P/Halley carry any traces of their origin in low velocity collisions? // The seventh Moscow Solar System symposium, 10-14 October 2016, Space Research Institute (IKI RAS), Moscow, p. 135, 7MS3-SB-07.

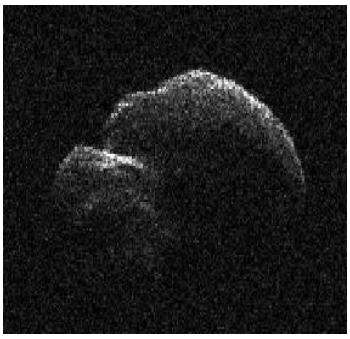
1

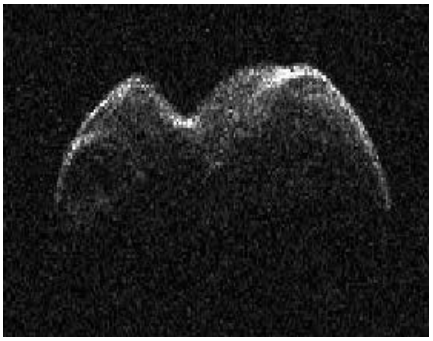
2

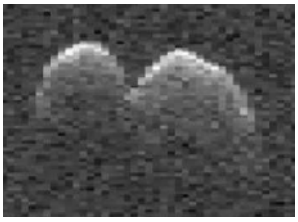
3

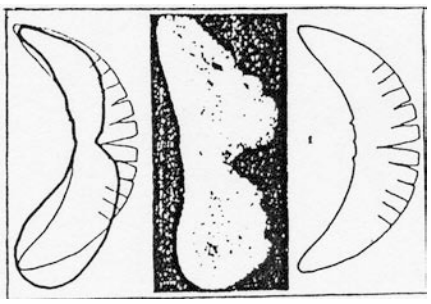
4

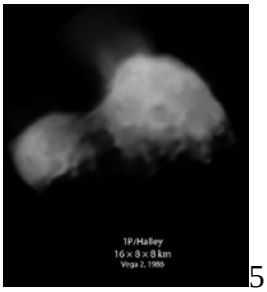

5

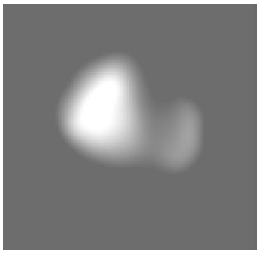
6

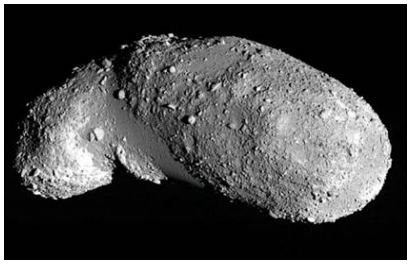
7


8

9

1, 2- Asteroid 2014J025, dimension ~870 m, Arecibo Observatory Planetary Radar System, 17-20 April 2017; **3-** Asteroid 1999JD6, 700_400985f8789ec19308d1b83b5a840ca9, PIA19647; **4-** Asteroid (433)Eros. 33 km long. NEAR image & a model of body bending, destruction and two-lobed shape formation; **5-** Comet 1P/Hailey, 16 x 8 x 8 km, Vega 2, 1986; **6-** Nix-satellites of Pluto; **7-** Asteroid {25143}Itokawa. 0.5 km long; **8-** Asteroid 4179Toutatis. Spectral type S. Chang'e 2 image. 4.75 x 2.4 x 1.95 km. Diameter 5.4 km, two halves 4.6 and 2.4 km; **9-** 67P/ Churyumov-Gerasimenko comet core , 4 x 3 km, Rosetta, 2014.

EPSC Abstracts
Vol. 11, EPSC2017-126, 2017
European Planetary Science Congress 2017

DEEP-South: Lightcurve Analysis of near Earth asteroids

M.-J. Kim (1), H.-K. Moon (1), J. Park (1), H.-J. Lee (1,2), Y.-J. Choi (1,3), H.-S. Yim (1), D.-G. Roh (1), and the DEEP-South Team
(1) Korea Astronomy and Space Science Institute, Korea, (2) Chungbuk National University, Korea, (3) University of Science and Technology, Korea (skarma@kasi.re.kr/ Fax: +82-42-865-3358)

Abstract

DEep Ecliptic Patrol of the Southern Sky (DEEP-South) [1] observation is being made during the off-season for exoplanet survey, using Korea Microlensing Telescope Network (KMTNet). KMTNet is a network of three identical 1.6 m wide-field telescopes equipped with 18K×18K mosaicked CCDs located in the southern hemisphere; Chile (CTIO), South Africa (SAAO), and Australia (SSO) [2]. An optimal combination of its prime focus optics and the 0.3 billion pixel CCD provides a four square degrees field of view with 0.4 arcsec/pixel plate scale. Normal operation of KMTNet started in October 2015, and a significant portion of the allocated telescope time for DEEP-South is dedicated to targeted observation, Opposition Census (OC) [1], of near-Earth asteroids for physical and taxonomic characterization. This is effectively achieved through multiband, time series photometry using Johnson-Cousins BVRI filters. We present the lightcurves and rotational properties of NEAs from the DEEP-South Project.

Facility

Korea Microlensing Telescope Network (KMTNet) is an array of wide-field optical telescopes, each consists of an identical 1.6 m prime focus optics and an 18k×18k CCD covering 4 square deg FOV. It is being operated at CTIO, SAAO, and SSO, providing 24-hour monitoring of the southern sky. Its wide FOV and the round-the clock operation capability enables discovery, astrometry and physical characterization of asteroids in an efficient way.

Observation mode

Part of the allocated time is used for targeted photometry of NEAs to increase the number of objects with known physical properties. It is achieved by multiband, time series photometry. The Opposition Census (OC) mode targets NEAs near opposition, with km-sized PHAs in an early stage and goes down to smaller ones in a later stage. We adopt R-band for lightcurve study, and BVI-bands for taxonomy and confirmation of possible color variations.

Network observation

Uninterrupted monitoring of the southern sky with this network of telescopes is optimized for spin characterization of a broad spectrum of asteroids ranging from the near-Earth space to the main-belt, including binaries, asteroids with satellites, slow/fast- and non-principal axis-rotators [3], and thus is expected to facilitate the debiasing of previously reported lightcurve observations. Our software subsystem consists of an automated observation scheduler, a pipelined data processing system for differential photometry, and an easy-to-use lightcurve analysis toolkit [4].

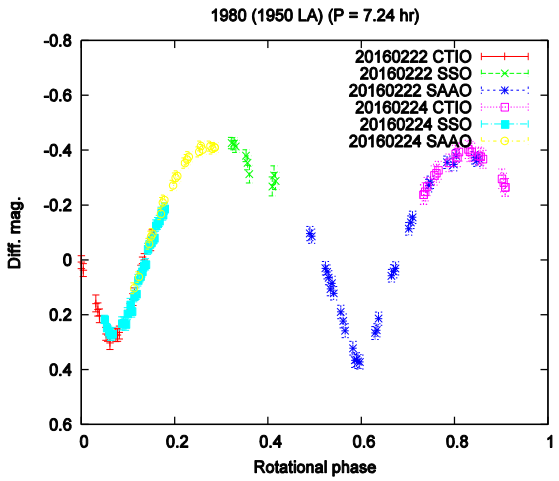

Figure 1: An example of asteroid lightcurve of 1980 Tezcatlipoca (1950 LA) obtained at three KMTNet stations in the southern hemisphere.

Acknowledgements

This work is supported by Korea Astronomy and Space Science Institute (KASI).

References

[1] Moon, H.-K., Kim, M.-J., Yim, H.-S., et al. (2016) IAUS, 318, 306-310.

[2] Kim, S.-L., Lee, C.-U., Park, B.-G., et al. (2016) JKAS, 49, 37-44.

[3] Lee, H.-J., Moon, H.-K., Kim, M.-J., et al. (2017) JKAS, submitted.

[4] Yim, H.-S., Kim, M.-J., Bae, Y.-H., et al. (2016) IAUS, 318, 311-312

EPSC Abstracts
Vol. 11, EPSC2017-137, 2017
European Planetary Science Congress 2017

NEOShield-2 project: Phase effects in NEA visible spectra

M. A. Barucci (1), D. Perna (1), I. Beskaya (2) M. Popescu (1, 3), S. Fornasier (1), A. Doressoundiram (1), C. Lantz (1, 4) , F. Merlin and (1) and M. Fulchignoni (1).

(1)LESIA, Observatoire de Paris, PSL Research University, CNRS, Univ. Paris Diderot, Sorbonne Paris Cité, UPMC Univ., Paris 06, Sorbonne Universités, 5 Place J. Janssen, Meudon Pricipal Cedex 92195, France (antonella.barucci@obspm.fr), (2) Institute of Astronomy, V.N. Karazin Kharkiv National University, 35 Sumska Str., 61022 Kharkiv, Ukraine, (3) Astronomical Institute of the Romanian Academy, 5 Cutitul de Argint, 040557 Bucharest, Romania, (4) EAPS-MIT, Cambridge, MA, USA.

Abstract

The analysis of about 180 spectral observations of 137 small Near Earth Asteroids, obtained in the framework of the NEOShield-2 project and made in a wide range of phase angles, allows to estimate phase reddening of the visible spectral slope (0.44-0.65 μm) for different asteroid types.

1. Introduction

In the framework of the NEOShield-2 observational campaign, we obtained about 180 new spectra for 137 small NEA objects. A number of 29 asteroids with diameters less than 100 meters and 71 with diameters between 100 m and 300 m were characterized (Perna et al., this issue).

The NEOShield-2 project has been funded by European Commission (2015-2017) in the framework of the EU H2020 program following the first NEOShield (2012-2015) which principal aim was to investigate the most promising mitigation techniques of an asteroid impact risk. One of the main objectives of the NEOShield-2 project is to provide physical and compositional characterization of a large number of NEOs in the hundred-meter size range. An extensive observational campaign involving complementary techniques was undertaken in Europe. Our team at LESIA is the leader of the entire observational program. Priority was given to potential space mission targets, optimized for mitigation or exploration missions

Spectral observations of NEAs are typically made at larger phase angles than main-belt asteroids and need to be corrected for the phase reddening effect before comparison of their spectra. According to [1] the increase in spectral slopes caused by phase reddening can be comparable to space weathering and could lead to an ambiguous taxonomic classification. Up to now our knowledge of phase reddening effect for NEAs is rather limited [2-4]. With our new spectral observations of 180 NEA spectra we make an attempt to estimate phase reddening of the visible spectral slope (0.44-0.65 μm).

2. Observation and results

Our team obtained a GTO program at ESO with an allocation of 30 observing nights at NTT telescope to characterize the composition of the small population of asteroids. Up to now we have obtained 180 spectra of NEOs for 137

objects. The observations were performed with EFOSC2 instrument at NTT telescope in the wide range of phase angles from 2 to 92 deg. We covered the wavelength interval 0.4-0.92, with a resolution of R=~200. We classified each spectrum by performing curve matching with the 25 classes defined by Bus-DeMeo taxonomy.

As a result of the limited spectral range we grouped together certain classes into broader complexes (C-, S-, and X-complex). For all observed objects we calculated the spectral slope in the range of 0.44-0.65 μm and found the phase-angle dependence within the particular type. The largest phase reddening is seen for the A and Q-types (Fig.1). Asteroids of the S-complex also show phase reddening but the data scatter is larger, probably because of less homogeneous composition.

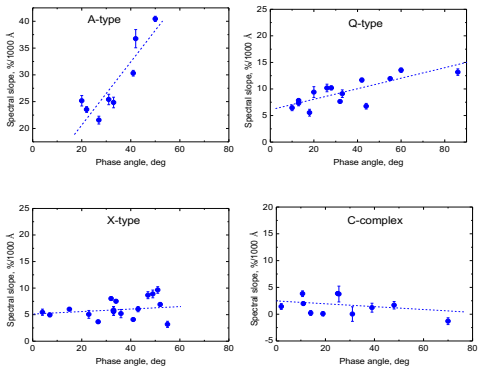

Figure 1: The phase reddening in the visible spectral slope (0.44-0.65 μm) for different asteroid types.

Conversely to silicate rich asteroids, the C-complex do not show phase reddening but hints of spectral blueing at large phase angle.

The dispersions in spectral slopes of the X-type asteroids at large phase angles can be explained by different phase angle behaviours for P, M, E-types.

3. Conclusions

The visible spectral slope of the measured NEAs revealed strong dependence on phase angle. The largest phase reddening is inherent for olivine-rich A and Q-type asteroids. We found a phase blueing for the C-complex asteroids. If blueing effect is confirmed, it will give a way to distinguish low albedo NEAs from the X-complex.

Acknowledgements

We acknowledge the financial support from the NEOShield-2 project, funded by the European Commission Horizon 2020 program (contract No. PROTEC-2-2014-640351) and from the French Planetology National Programme (INSU-PNP).

References

[1] Sanchez, J.A., Reddy, V., Nathues, A. et al.: Phase reddening on near-Earth asteroids: Implications for mineralogical analysis, space weathering and taxonomic classification, Icarus, Vol. 220, pp. 36-50, 2012.

[2] Carvano, J.M., and Davalos, J.A.G.: Shape and solar phase angle effects on the taxonomic classification of asteroids. Astron. Astroph., Vol. 580, A98, 2015.

[3] Luu, J.X. and Jewitt, D.C.: Charge-coupled device spectra of asteroids. I. Near-Earth and 3:1 resonance asteroids. Astron. J., Vol.99, pp.1985-2011, 1990.

[4] Michelsen, R., Nathues, A., Lagerkvist, C.-I.: Spectroscopy of near-Earth asteroids. Astron. Astroph., Vol. 451, pp.331-337, 2006.

EPSC Abstracts
Vol. 11, EPSC2017-160, 2017
European Planetary Science Congress 2017

The Cost-Effective and Efficient Asteroid Taxonomy for Classification Using Johnson-Cousins BVRI Colors

D.-G. Roh (1), **H.-K. Moon (1)**, M.-S. Shin (1), H.-J. Lee (1, 2), M.-J. Kim (1), and DEEP-South Team, (1) Korea Astronomy and Space Science Institute, Korea, (2) Chungbuk National University, Korea (fullmoon@kasi.re.kr/ Fax: +82 42 861 5610)

Abstract

It is a tradition that taxonomic classes of asteroids are grouped and divided into broad complexes based on visual and near-infrared spectroscopy: silicates (S), carbonaceous (C), featureless (X), Vestoids (V), and the end-members that do not fit well within the S, C, X and V complexes. The extension of the scheme was recently established using the SDSS 4th Moving Object Catalog (MOC 4). However, the boundaries of each major complex and their subclasses have been inevitably ill-defined. Further, there are only few studies on asteroid taxonomy in Johnson-Cousins photometric bands by using a small number of objects with non-negligible measurement uncertainties although these bands are most commonly used. In this paper, we present our results on a novel taxonomic classification system of asteroids using archived data. We determine the class centers and boundaries of each taxonomy complex in a statistically robust way. Our tests of two different clustering methods reveal well-defined taxonomy complexes in the three dimensional Johnson-Cousins color spaces, confirming that our new scheme is very effective.

1. Introduction

To date, different taxonomy classes of asteroids have been characterized by spectral slopes shortward of 0.75 μm and the absorption band at 1 μm using ~10^3 spectra [1][2][3]. In the meantime, we witnessed an explosion of observation data with ~10^5 photometric colors attributed to large-scale surveys such as Sloan Digital Sky Survey (SDSS) [4]. This resulted in an extended taxonomic classification of asteroids to the SDSS Moving Object Catalogue 4 (MOC4) [5]. The class boundaries of each taxonomic complex and the subclass are somewhat ambiguously defined by the extended scheme in the traditional two dimensional plane which comprises the spectral slope and 1-μm absorption depth, or their corresponding 2-D-colors. We present a new solution to the long-standing issue with this classical approach for taxonomical classification of asteroids.

2. Datasets

We make use of ~400 visual-NIR reflectance spectra [6] and ~4200 MOC4 [5] photometric colors which are converted to Johnson-Cousins system for objects with photometric errors < 0.05 mag, and galactic latitude |b| > 15 deg. at the time of observations. In addition, ~1400 Johnson-Cousins band colors are estimated from the SMASS (Small Main-belt Asteroid Spectroscopic Survey) database [2].

3. From 2-D spectra to 3-D colors

We establish a three dimensional coordinate system for asteroid taxonomy taking 1) Johnson-Cousins (B-V) color for spectral slope, 2) (R-I) color for the depth of the 1-μm band, and 3) (B-V) + (B-R) + (B-I) colors as the third axis roughly corresponds to the total area of the, normalized at Johnson-Cousins B-band center.

4. 3-D Clustering method

We utilize two clustering methods to identify major taxonomic types in the 3-dimensional color space. Our methods describe the distribution of asteroid colors as mixtures of 3-D Gaussian distributions. The method 1 estimates properties of these Gaussian mixtures in terms of an Infinite Gaussian Mixture model [7], [8] without any prior information of known asteroid types and their colors in the input data. In the meanwhile, the method 2 uses the DeMeo & Carry dataset [6] with known taxonomy types as well as the synthetic color distribution in the 3-D color space, assuming that we have a sufficient number of sample asteroids for the known taxonomy types in the input data. The cluster membership is accurately determined by distance from the centers of found mixture in the 3-D Johnson-Cousins color space, as well as the probability of assignment to the found mixture components.

5. Future works

This classification scheme is considered to be the cost-effective, efficient, and reliable method of asteroid taxonomy. We plan to test our 3-D clustering techniques to further revise estimation of each complex and subclass boundaries. To achieve this, we will collect more photometric and spectroscopic data to increase the size of the reference input data (i. e., samples with known types in the 3-D color space). Furthermore, in the years to come, we will extend the work to prepare in advance for the "LSST-GAIA era", using the LSST pass bands and the GAIA low resolution spectra.

Acknowledgements

This work is supported by Korea Astronomy and Space Science Institute (KASI).

References

[1] Tholen, D. J.: Doctoral Thesis, University of Arizona, 1984.

[2] Bus, S. J. and Binzel, R. P.: Icarus, Vol. 158, pp. 146–177, 2002.

[3] DeMeo, F. E. et al.: Icarus, Vol. 202, pp. 160–180, 2009.

[4] Ivezic, Z. et al.: AJ, Vol. 134, pp. 331–334, 2002.

[5] Juric, M. et al.: AAS, #211,7-11 January 2008, Austin, Texas, 2008.

[6] DeMeo, F. E. and Carry, B.: Icarus, Vol. 226, pp. 723–741, 2013.

[7] Shin, M.-S. et al.: MNRAS, Vol. 400, pp. 1897-1910, 2009

[8] Shin, M.-S. et al.: AJ, Vol. 143, pp. 65-92, 2012

EPSC Abstracts
Vol. 11, EPSC2017-220, 2017
European Planetary Science Congress 2017

The "small" NEA population: results of a spectroscopic survey in the framework of the NEOShield-2 project

D. Perna (1,2) and the NEOShield-2 Team
(1) INAF – Osservatorio Astronomico di Roma, Italy, (2) LESIA – Observatoire de Paris, France (davide.perna@oa-roma.inaf.it / davide.perna@obspm.fr)

Abstract

One of the main aims of the NEOShield-2 project, financed in 2015-2017 by the European Commission in the framework of the H2020 program, is to undertake a comprehensive investigation of the physical properties of the "small" near-Earth asteroid (NEA) population. Here we report the results of a visible spectroscopic survey of 137 small (H≥20) NEAs, performed in the framework of NEOShield-2. These data significantly increase the available literature in this size range, and show a peculiar distribution of spectral types for such small NEAs.

1. Introduction

The impacts of small asteroids may have played an important role in the emergence of life on our planet, with the "gentler" delivery of water and organics to the early Earth [e.g., 9]. Moreover, objects in the few-hundred-meter size range might represent the most probable hazard in the near future, with impact frequencies of the order of ~10^3 yrs and sizes large enough to cause extensive damage at regional level in the event of impact [e.g., 7].

In the framework of the NEOShield-2 project, we managed a 30-night Guaranteed Time Observations (GTO) programme at the ESO-NTT telescope (La Silla, Chile). Visible spectroscopic observations were performed between April 2015 and February 2017, using the EFOSC2 instrument, to undertake – for the first time ever – a comprehensive characterization of the surface properties of the small NEA population.

2. Data Analysis

We obtained good quality spectra of 137 NEAs with absolute magnitude H≥20. We classified each spectrum by performing curve matching with the visible part of the classes defined by the Bus-DeMeo taxonomy [4], using the M4AST webtool [10]. Because of the limited spectral range (0.4-0.92 μm) available, we grouped together certain classes into broader complexes (C-complex, S-complex, X-complex). The few data available in the literature for these objects (i.e. 10 objects have NIR spectra and the albedo is known for six of them) confirm our classification.

The distribution of the equivalent diameters of our targets – computed by taking into account the mean albedo [6] of the assigned taxonomic class – is reported in Fig. 1. Twenty-nine NEAs with diameters smaller than 100 m (more than the double of the previous literature for this size range) and 71 with diameters in the range 100-300 m were characterized.

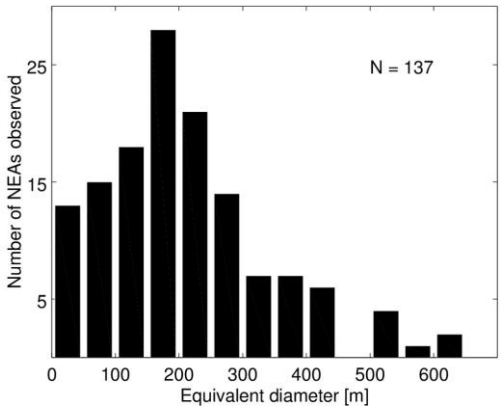

Figure 1: Distribution of the sizes (shown as equivalent diameter) of the observed NEAs.

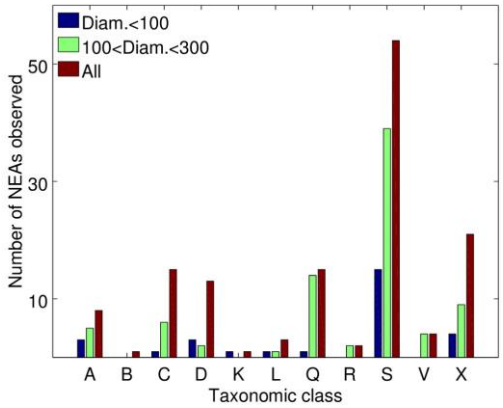

Figure 2: Taxonomical types distribution of the observed NEAs. The distribution of objects smaller than 100 m, and of objects with diameter between 100 m and 300 m, are shown separately.

3. Results and Conclusions

The taxonomic distribution of the observed NEAs is shown in Fig. 2. This distribution is dominated by the S-complex (Sq-, Sr-, Sv- and S-types) at all sizes.

Compared with the literature studies of larger NEAs [e.g.: 2,8], we note the relative abundance within the small NEA population of rare taxonomical types: we found 8 olivine-rich A-types, as well as 13 primitive (organics- and volatiles-rich) D-types.

The large majority of the Q-types we identified (13 out of 14 objects), which are associated to a resurfacing of S-type asteroids during close approaches with terrestrial planets [3,5], have a size larger than 100 meters.

Our observations, spanning solar phase angles in the range 2-92 degrees, allowed us to evidence distinctive phase reddening for different spectral types [1].

Acknowledgements

We acknowledge the financial support from the NEOShield-2 project, funded by the European Commission's Horizon 2020 program (contract No. PROTEC-2-2014-640351).

References

[1] Barucci, M. A., Perna, D., Belskaya, I., et al.: NEOShield-2 project: Phase effects in NEAs visible spectra, this issue.

[2] Binzel, R. P., Rivkin, A. S., Stuart, J. S., et al.: Observed spectral properties of near-Earth objects: results for population distribution, source regions, and space weathering processes, Icarus, 170, 259 (2004).

[3] Binzel, R. P., Morbidelli, A., Merouane, S., et al.: Earth encounters as the origin of fresh surfaces on near-Earth asteroids, Nature, 463, 331 (2010).

[4] DeMeo, F. E., Binzel, R. P., Slivan, S. M., and Bus, S. J.: An extension of the Bus asteroid taxonomy into the near-infrared, Icarus, 202, 160 (2009).

[5] DeMeo, F. E., Binzel, R. P., and Lockhart, M.: Mars encounters cause fresh surfaces on some near-Earth asteroids, Icarus, 227, 112 (2014).

[6] Mainzer, A., Grav, T., Masiero, J., et al.: NEOWISE Studies of Spectrophotometrically Classified Asteroids: Preliminary Results, ApJ, 741, 90 (2011).

[7] Perna, D., Barucci, M. A., Drube, L., et al.: A global response roadmap to the asteroid impact threat: The NEOShield perspective, P&SS, 118, 311 (2015).

[8] Perna, D., Dotto, E., Ieva, S., et al.: Grasping the Nature of Potentially Hazardous Asteroids, AJ, 151, 11 (2016).

[9] Pierazzo, E. and Chyba, C. F.: Amino acid survival in large cometary impacts, M&PS, 34, 909 (1999).

[10] Popescu, M., Birlan, M., and Nedelcu, D. A.: Modeling of asteroid spectra - M4AST, A&A, 544, A130 (2012).

EPSC Abstracts
Vol. 11, EPSC2017-302, 2017
European Planetary Science Congress 2017

Shock-darkening in ordinary chondrites: Modeling of the pressure-temperature conditions

J. Moreau (1), T. Kohout (1,2) and K. Wünnemann (3)
(1) Department of Physics, University of Helsinki, Finland, (juulia.moreau@helsinki.fi) (2) Institute of Geology, The Czech Academy of Sciences, Prague, Czech Republic, (3) Museum für Naturkunde, Leibniz Institute for Evolution and Biodiversity Science, Berlin, Germany

Abstract

Shock-darkening in ordinary chondrites is the melting of iron sulfides and metals into a network of veins rendering the lithology darker. Using the shock physics code iSALE [7, 8] we determined the shock-darkening pressure range to be 40-50 GPa for the melting of iron sulfides. Modeling and thermal effect uncertainties are also discussed in our work.

1. Introduction

Shock-darkening in ordinary chondrites is the partial melting of metals and iron sulfides filling cracks within silicate grains [5]. It leads to optical darkening and makes asteroid classification more difficult [2, 3]. In such cases, S-type asteroids (chondritic silicate composition) spectra look like C-type asteroids (associated with carbonacaeous chondrites).

2. Methods

To study the pressure and temperature conditions at which this process occurs, we used the shock physics code iSALE [7, 8]. In our mesoscale models of a planar shock wave in 2D we study the complex interaction of shock wave with different mineral phases. We employ a model setup analogous to the setup in experiments: a flyer plate impacts a top buffer plate, which transmits the generated shock wave into the sample plate. A buffer plate at the bottom avoids boundary problems. All layers are composed of olivine. The pressure in the buffer plate is considered as nominal pressure. The sample plate contains also iron and troilite grains to mimic ordinary chondrites type H, L and LL composition.

The thermodynamic behaviour of olivine is described by ANEOS (analytical equation of state) with a porosity of 6% ([8], ε-α compaction model). Iron is described by ANEOS and Troilite by the Tillotson EOS (using pyrrhotite [1]).

To study melting, we use the peak shock pressures recorded in tracers, which can be translated into post-shock temperatures [4]. This approach assumes a constant heat capacity and heat of fusion is neglected. The total amount of melting is approximated by the ratio of tracers in a material reaching temperatures above the solidus and all tracers. This technique provides reasonable temperature estimates but suffers from several uncertainties (e.g. a positive ~10% error in pressure to reach melting point in troilite).

3. Results

We conducted models with each type of ordinary chondrites (H, L and LL). The iron/troilite particles distribution are according to data from [6]. Fig. 1 shows profiles of the tracer fractions reaching melt temperatures in the materials. We observe that:

- The onset of melting of troilite tracers occurs at ~40 GPa. At 52 GPa of nominal pressure all tracers reach melting point. It is a consequence of shock wave-induced increase in entropy (pure shock melting). This is only slightly influenced by reflexions when reaching peak shock pressures.

- In iron, only a few percents of tracers reach melting point at 58 GPa of nominal pressure. It is mainly due to strong reflections and specific disposition of the iron particles.

- Olivine tracers reach melting point at ~50 GPa of nominal pressure. This is due to strong reflexions of the shock wave at iron grains

boundaries, ramping up the peak shock pressures and, thus, post-shock temperatures.

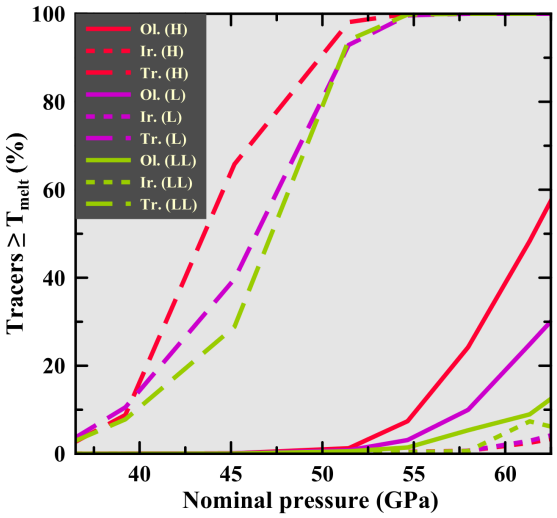

Figure 1: Results of the mesoscale models with porous olivine showing fractions of tracers reaching melting point in all materials after pressure release in each ordinary chondrite type. Each ordinary chondrite type is represented by its abbreviation and phases are Ir.: iron, Tr.: troilite, Ol.: olivine.

4. Discussion

Our results show that shock-darkening likely happens at pressures from 40 GPa to 50 GPa with almost all tracers in troilite reaching the melting point. Fractions of olivine start to reach melting point at 50 GPa. We observe that the influence of iron is important for the melting of olivine. The shock-darkening agent is only composed of troilite. In our models we did neither consider heat transfer nor the Fe-FeS eutectic point (unshocked petrologies show only few Fe-FeS mixtures) - melting temperatures for the materials were therefore high. No shearing between grains was considered. In general, the thermal and mechanical effects that are not taken into account in the modeling would eventually balance out with the uncertainties in estimating the post-shock temperature of the material (constant heat capacity and assuming that peak shock pressures represent single shocks).

5. Conclusions

Based on numerical modeling, the shock-darkening process in ordinary chondrites starts at ~40 GPa up to ~50 GPa. In each ordinary chondrite type, all troilite material reaches the melting point at ~52 GPa and is considered to be the darkening agent. Despite uncertainties in assessing the post-shock temperature giving a positive ~10% error in the required melt pressures estimate for troilite, heat transfer, shearing between grains, pores crushing, and the eutectic point are important aspects that we intend to investigate further in future.

Acknowledgements

Our thanks go to the team of the Museum für Naturkunde in Berlin, Germany, for sharing their knowledge and ideas with us. This work is also supported by the Academy of Finland.

References

[1] Ahrens. T. J. 1979. Equations of state of iron sulfide and constraints on the sulfur content of the Earth. Journal of Geophysical Research 84(B3):985-998.

[2] DeMeo F. E. and Carry B. 2014. Solar System evolution from compositional mapping of the asteroid belt. Nature, 505:629-634.

[3] DeMeo F. E., Binzel R. P., Slivan S. M. and Bus S. J. 2009. Extension of the Bus asteroid taxonomy into the near-infrared. Icarus, 202:160–180.

[4] Fritz J., Artemieva N. and Greshake A. 2005. Ejection of Martian meteorites. Meteoritics & Planetary science, 40(9/10):1393-1411.

[5] Kohout T., Gritsevich M., Grokhovsky V. I., Yakokiev G. A., Haloda J., Halodova P., Michallik R. M., Penttilä A. and Muinonen K. 2014. Mineralogy, reflectance spectra, and physical properties of the Chelyabinsk LL5 chondrite - Insight into shock-induced changes in asteroid regoliths. Icarus 228:78–85, DOI:10.1016/j.icarus.2013.09.027.

[6] McSween Jr. H. Y., Bennett III. M. E. and Jarosewich E. 1991. The mineralogy of ordinary chondrites and implications for asteroid spectrophotometry. Icarus, 90(1):107–116.

[7] Moreau J., Kohout T. and Wünnemann K. 2017. Shock-darkening in ordinary chondrites: pressure-temperature conditions determination by shock physics mesoscale modeling. Meteoritics & Planetary Science, submitted.

[8] Wünnemann K., Collins G. and Melosh H. 2006. A strain-based porosity model for use in hydrocode simulations of impact and implication for transient crater growth in porous targets. Icarus, 180:514-527.

EPSC Abstracts
Vol. 11, EPSC2017-341-1, 2017
European Planetary Science Congress 2017

The peculiar albedos of near-Earth and Mars-crossing asteroids: implications for the near-Earth object impact prevention and the NEOShield2 project

M. Delbo (1), V. Ali-Lagoa (2)
(1) Université Côte d'Azur, Observatoire de la Côte d'Azur Lagrange, CNRS, France.
(2) Max-Planck-Institut für extraterrestrische Physik, Giessenbachstrasse, Postfach 1312, 85741 Garching, Germany.
(delbo@oca.eu. / Fax: +33-4-92003028)

Abstract

Here we show that the albedo distributions of near-Earth and Mars-crossing asteroids are different. We explain these difference in terms of origin and fate of the near-Earth asteroids.

1. Introduction

The understanding of the origin, sizes, composition, internal structure of sub-kilometre-sized near-Earth asteroids (NEAs) is an important goals of planetary sciences. This is also one of the central questions that the projects NEO-Shield [1] and NEO-Shield2, funded by the H2020 program of the European Union, want to address. This knowledge will lead to better estimates of physical quantities of the NEA population, which are required to better assess the impact risk that NEAs pose to our planet [2]. In addition, this information is required to develop techniques to mitigate the potential damage produced by an asteroid, in case a collision with an NEA is deemed probable.

2. Origin of near-Earth asteroids

It is well understood that NEAs are on orbits which are unstable for periods longer than about 10My. Yet, NEAs existed over the age of the Solar System. Members of the NEA population must be thus constantly resupplied by the so-called NEA source regions [3]. Most of these regions are located in the Main asteroid Belt, but an additional important source is the population of Mars-crossing asteroids.

3. Mars- & Earth-crossing asteroid albedos

We recently determined the diameters and albedos of more than 1500 Mars-crossing asteroids (MCs) [4] from thermal modelling (using the NEATM; [5]) of infrared observations obtained by the WISE/NEOWISE mission [6, 7], including those taken for +300 objects during the fully cryogenic phase that had not been modelled before.

4. Results

The albedo (p_V) distribution of MCs shows the classical double peak: one peak centred at $p_V \sim 0.05$ and a second at $p_V \sim 0.25$ corresponding to the bulk of the asteroids belonging to the C- and the S- spectroscopic complexes respectively [8, 9] (Fig. 1).

On the other hand, the p_V-distribution of NEAs (which albedos were obtained from the literature) does not show this double peak (Fig. 1). An excess of asteroids with $0.1 < p_V < 0.2$ and a deficit of low-albedo objects is visible in the NEA population compared to that of the MCs. In this work we study the origin of these differences and their implications for the origin of NEAs.

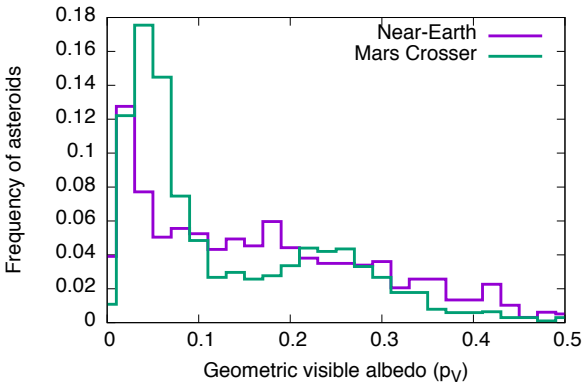

Figure 1: The albedo distributions of Mars-crosser and near-Earth asteroids

Acknowledgements

The results described here have been made possible by the NEOShield-2 project, which has received funding from the European Union's Horizon 2020 research and innovation programme under grant agreement No 640351. This research has made use of data and/or services provided by the International Astronomical Union's Minor Planet Center. This publication makes use of data products from NEOWISE, which is a project of the Jet Propulsion Laboratory/California Institute of Technology, funded by the Planetary Science Division of the National Aeronautics and Space Administration. This research also made use of the NASA/IPAC Infrared Science Archive, which is operated by the Jet Propulsion Laboratory, California Institute of Technology, under contract with the National Aeronautics and Space Administration.

References

[1] A W Harris, M A Barucci, J L Cano, A Fitzsimmons, M Fulchignoni, S F Green, D Hestroffer, V Lappas, W Lork, P Michel, D Morrison, D Payson, and F Schäfer. The European Union funded NEOShield project: A global approach to near-Earth object impact threat mitigation. *Acta Astronautica*, 90(1):80–84, September 2013.

[2] A W Harris, M Boslough, C R Chapman, L Drube, and P Michel. Asteroid Impacts and Modern Civilization: Can We Prevent a Catastrophe? *Asteroids IV*, pages 835–854, 2015.

[3] Mikael Granvik, Alessandro Morbidelli, Robert Jedicke, Bryce Bolin, William F Bottke, Edward Beshore, David Vokrouhlický, Marco Delbo, and Patrick Michel. Supercatastrophic disruption of asteroids at small perihelion distances. *Nature*, 530(7):303–306, February 2016.

[4] Victor Ali-Lagoa and Marco Delbo. Sizes and albedos of Mars-crossing asteroids from WISE/NEOWISE data. *Astronomy and Astrophysics*, pages 1–8, February 2017.

[5] Alan W Harris. A Thermal Model for Near-Earth Asteroids. *Icarus*, 131(2):291–301, February 1998.

[6] A Mainzer, T Grav, J Bauer, J Masiero, R S McMillan, R M Cutri, R Walker, E Wright, P Eisenhardt, D J Tholen, T Spahr, R JEDICKE, L Denneau, E DeBaun, D Elsbury, T Gautier, S Gomillion, E Hand, W Mo, J Watkins, A Wilkins, G L Bryngelson, A Del Pino Molina, S Desai, M Gómez Camus, S L Hidalgo, I Konstantopoulos, J A Larsen, C Maleszewski, M A Malkan, J C Mauduit, B L Mullan, E W Olszewski, J Pforr, A Saro, J V Scotti, and L H Wasserman. NEOWISE Observations of Near-Earth Objects: Preliminary Results. *The Astrophysical Journal*, 743(2):156, December 2011.

[7] A Mainzer, F Usui, and D E Trilling. Space-Based Thermal Infrared Studies of Asteroids. *Asteroids IV*, pages 89–106, 2015.

[8] F E DeMeo and B Carry. The taxonomic distribution of asteroids from multi-filter all-sky photometric surveys. *Icarus*, 226(1):723–741, September 2013.

[9] F E DeMeo, C M O'D Alexander, K J Walsh, C R Chapman, and R P Binzel. The Compositional Structure of the Asteroid Belt. *Asteroids IV*, pages 13–41, 2015.

EPSC Abstracts
Vol. 11, EPSC2017-379, 2017
European Planetary Science Congress 2017

Dynamically interesting asteroids discovered at the VATT Observatory

I. Wlodarczyk (1), K. Cernis (2) and **R. Boyle** (3)
(1) Chorzow Astronomical Observatory (IAU 553), Al. Planetarium 4, Chorzow 41-500, Poland (e-mail:astrobit@ka.onet.pl), (2) Institute of Theoretical Physics and Astronomy, Vilnius University, Goštauto 12, Vilnius LT-01108, Lithuania (e-mail:Kazimieras.Cernis@tfai.vu.lt), (3) Vatican Observatory Research Group, Steward Observatory,Tucson,Arizona 85721, U.S.A. (e-mail:rpboyle@mac.com)

Abstract

We present results of a long-term research program on dynamically interesting asteroids discovered at the VATT Observatory.

1. Introduction

One of the research projects of the Vatican Observatory is a study of asteroids for a better prediction of their orbits. The observing program on the 1.8 m telescope VATT is targeted on observing the Main Belt and the Centaur group asteroids, Trans-neptunian objects (TNO), as well as on the search of new objects. First astrometric observations of asteroids and comets with the VATT at the Mt. Graham Observatory (IAU code 290, longitude 109.89201 W, latitude 32.70133 N, altitude 3178 m) were initiated in 2000-2001 using CCD images exposed in the focal plane of the VATT [1].

The first new asteroid, (220696) = 2000 YJ143, was discovered in 2000 by W. H. Ryan. In 2007, 75 new asteroids were discovered by C. W. Hergenrother. A new observational program for the search and observations of asteroids was started in 2009 by R. P. Boyle and K. Černis.

2. Orbits

We continue presentation of dynamically interesting asteroids discovered at the VATT Observatory. They are described in:

→Centaur Asteroid 2012 DS85 [5]

→Amor-class asteroid 2012 XH16 [6]

→Transneptunian (TNO) object (420356) 2012 BX85 Praamžius [7]

→Distant Object (463368) 2012 VU85 [8]

Fig. 1 presents orbits of four discovered asteroids at VATT Observatory in the ecliptic plane: 2012 DS85, 2012 XH16, (420356) 2012 BX85 Praamžius and (463368) 2012 VU85.

The first object observed was an asteroid of the Centaur group 2009 HW77 [2],[4] in April of 2009. All published orbits of asteroids discovered at the VATT Observatory were computed by I. Wlodarczyk using the OrbFit software (http://adams.dm.unipi.it/∼orbmaint/orbfit/). Accuracy of computations is described in [3].

3. Summary and Conclusions

We presented short history of asteroids discovered at the VATT Observatory. Starting orbits of four selected asteroids are presented in Fig. 1.

References

[1] Hergenrother C.W. and Spahr T.B. 2001, MPC 42751

[2] Černis K., Eglitis I., 2009, MPEC, 2009-U68

[3] Wlodarczyk I., 2009, Icar, 203, 119

[4] Wlodarczyk I., Cernis K., Eglitis I., 2011, MNRAS, 418, 2330

[5] Černis K., Boyle R. P., Laugalys V., Wlodarczyk I., 2012, BaltA, 21, 455

[6] Wlodarczyk I., Cernis K., Boyle R. P., Laugalys V., 2014, MNRAS, 438, 2621

[7] Černis K., Boyle R. P., Wlodarczyk I., 2016, BaltA, 25, 189

[8] Wlodarczyk I., Černis K., Boyle R. P., 2017, AcA, 67, 81

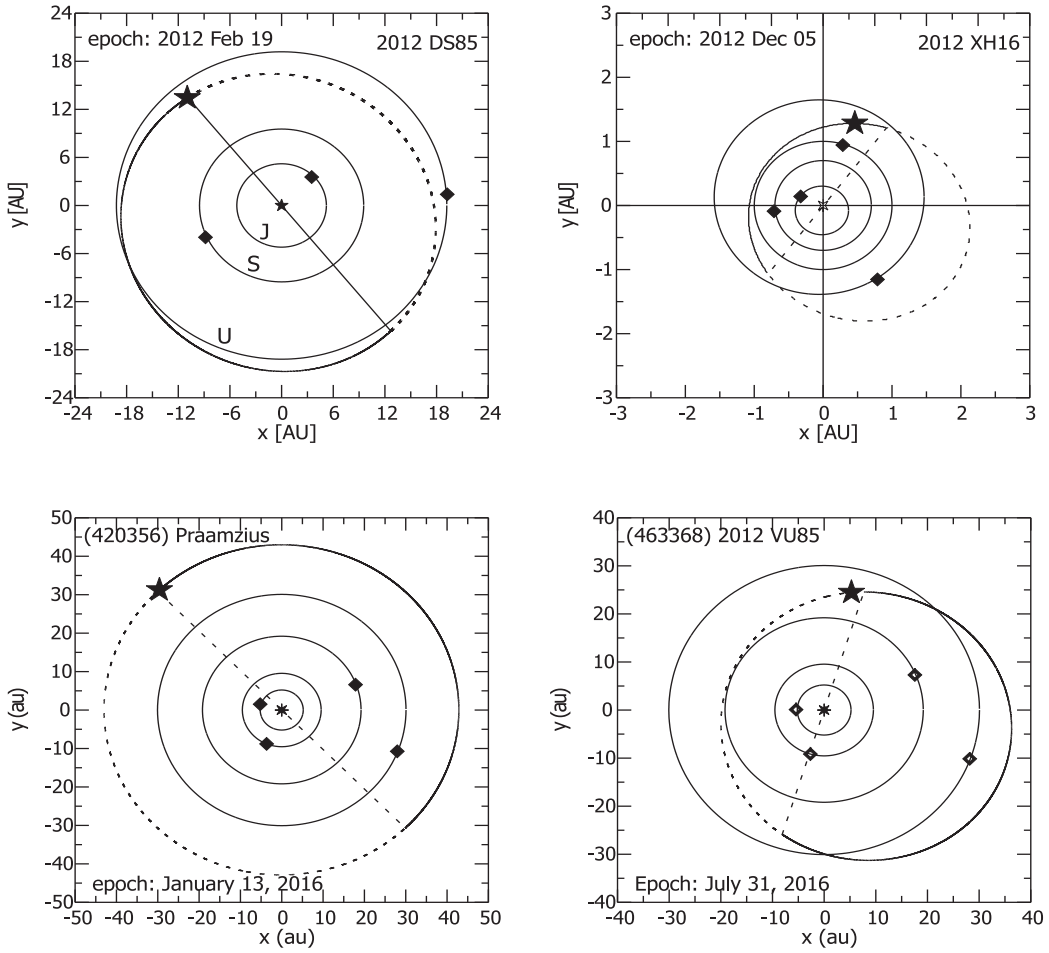

Figure 1: Orbits of selected asteroids discovered at VATT Observatory presented in the ecliptic plane. The dashed line denotes the part of the orbit below the ecliptic plane.

EPSC Abstracts
Vol. 11, EPSC2017-465, 2017
European Planetary Science Congress 2017

Thermal and tidal destruction of near-Earth objects

M. Granvik (1) and K. J. Walsh (2)
(1) Department of Physics, P.O. Box 64, 00014 University of Helsinki, Finland (mgranvik@iki.fi)
(2) Southwest Research Institute, 1050 Walnut St., Ste 300, Boulder, CO 80302, USA

Abstract

The general assumption for the fate of near-Earth objects (NEOs) was that most of them plunge into the Sun [1], roughly a quarter are cleared by Jupiter, and the remaining few percent impact the terrestrial planets, most often the Earth. A more complex picture for the fate of NEOs is starting to emerge as a result of efforts to understand the debiased orbit and absolute magnitude distributions for NEOs. Two particularly interesting phenomena are the thermal destruction of asteroids at small perihelion distances and the tidal disruption of asteroids during close encounters with terrestrial planets. It is likely that detailed physical modeling of these phenomena will allow us to place useful constraints on asteroid bulk composition and interior structure using data from, primarily, ongoing (e.g., Catalina Sky Survey, Panoramic Survey Telescope And Rapid Response System) and planned NEO surveys (e.g., Large Synoptic Survey Telescope).

1. Thermal destruction

By comparing predicted distributions of near-Earth-object (NEO) orbits and absolute magnitudes with observations by the CSS during 2005–2012 it was recently shown that there are up 10x fewer NEOs observed than predicted on orbits with small perihelion distances. The only way to reconcile the discrepancy is to assume that most NEOs are destroyed when reaching small, yet non-trivial distances from the Sun [2]. The (primary) physical mechanism causing these super-catastrophic disruptions is still undefined but it is most likely thermally driven. The most obvious alternatives have already been ruled out (Fig. 1).

2. Tidal disruption

It has been proposed that some (small) fraction of NEOs may be tidally disrupted during close encounters with terrestrial planets [3], although this has so far not been backed up by population-wide observational evidence. See [4] for evidence for a possible tidal re-shaping of (1620) Geographos. Further analysis of the distribution of perihelion distances [2] shows that the model underoverpredicts the number of NEOs with perihelion distance coinciding with the semimajor axes of Venus and the Earth (Fig. 2). This agrees with the prediction for tidal disruptions [5, 6] and cannot be explained by selection effects or orbital dynamics.

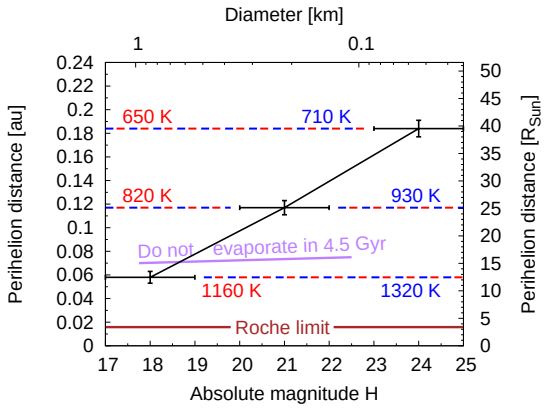

Figure 1: The typical disruption distance as a function of NEO size based on model fits to observed NEO population [2]. The horizontal dashed lines show estimated ranges for surface temperature. Direct evaporation and tidal disruption during close encounters with the Sun are ruled out as disruption mechanisms.

Acknowledgements

MG is supported by grant #299543 awarded by the Academy of Finland.

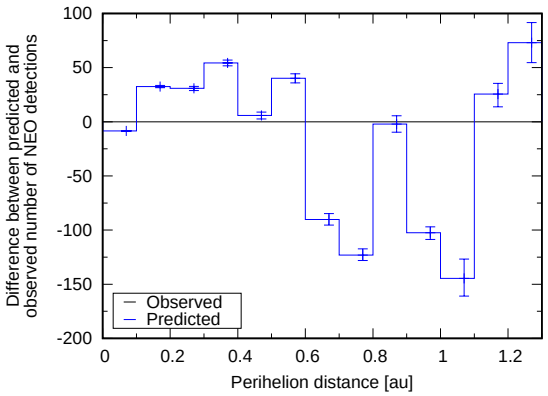

Figure 2: Difference between predicted and observed number of NEO detections by CSS as a function of perihelion distance. The prediction assumes a super-catastrophic and thermally-driven disruption when the perihelion distance reaches below 0.076 au [2] but it does not account for tidal disruptions. The same observed excess at the semimajor axes of Venus (∼0.7 au) and the Earth (∼1 au) is also seen for models not accounting for thermally-driven disruption.

References

[1] Farinella, P., Froeschlé, Cr., Froeschlé, Cl., Gonczi, R., Hahn, G., Morbidelli, A., and Valsecchi, G.: Asteroids falling into the Sun, Nature, 371, 314–317, 1994.

[2] Granvik, M., Morbidelli, A., Jedicke, R., Bolin, B., Bottke, W. F., Beshore, E., Vokrouhlický, D., Delbó, M., and Michel, P.: Super-catastrophic disruption of asteroids at small perihelion distances, Nature, 530, 303–306, 2016.

[3] Richardson, D. C., Bottke, W. F., and Love, S. G.: Tidal Distortion and Disruption of Earth-Crossing Asteroids, Icarus, 134, 47–76, 1998.

[4] Bottke, W. F., Richardson, D. C., Michel, P., and Love, S. G.: 1620 Geographos and 433 Eros: shaped by planetary tides?, AJ, 117, 1921–1928, 1999.

[5] Schunova, E., Jedicke, R., Walsh, K. J., Granvik, M., Wainscoat, R. J., and Haghighipour, N.: Properties and evolution of NEO families created by tidal disruption at Earth, Icarus, 238, 156–169, 2014.

[6] Walsh, K. J., Granvik, M., and Richardson, D. C.: Tidal Disruption — New Limits on Disruption and Bifurcated Shapes, Asteroids, Comets, Meteors 2017, 9–14 April 2017, Montevideo, Uruguay, 2017.

EPSC Abstracts
Vol. 11, EPSC2017-489-2, 2017
European Planetary Science Congress 2017

Duration of temporary capture of asteroids around an eccentric planet

A. Higuchi (1), S. Ida (2) and T. Tanigawa (3)
(1) Tokyo Institute of Technology, Tokyo, Japan, (2) Earth-Life Science Institute, Tokyo Institute of Technology, Tokyo, (3) National Institute of Technology, Ichinoseki College, Ichinoseki, Japan (higuchia@geo.titech.ac.jp)

Abstract

We have investigated the temporary capture of asteroids by an eccentric planet. We performed numerical orbital integrations and examined the duration of temporary capture. We found that the distributions of the duration of temporary capture for prograde and retrograde captures are different. The distributions can be described by a broken power law. The parameters to characterize the distributions are functions of the type of capture, the incident velocity to the Hill sphere, and the mass and eccentricity of the host planet.

1. Introduction

Irregular satellites around giant planets, which are small with elliptical and inclined orbits, are usually thought to be passing asteroids that were captured (e.g., [1]). The objects that are temporarily captured in the Hill sphere of a planet can become permanently captured due to some energy loss (e.g., tidal dissipation, drag force from a circumplanetary disk when it existed, or collisions with other solid bodies in the disk). Higuchi & Ida (2017)[2] derived the conditions for the temporary capture by an eccentric planet in an elliptic orbit as functions of the mass and eccentricity of the host planet. However, they didn't discuss temporary capture time, which could be an important factor in the evolution toward permanent capture. In this paper, we show the results of numerical orbital integrations focusing on the lifetime of the test particles as temporarily captured satellites. This is done in order to discuss the origins of general irregular satellites of planets, especially those of Mars.

2. Numerical Calculations

We perform numerical calculations for the temporary capture of bodies by planets with Mars, Jupiter, Earth, and Neptune masses. We compute the orbital evolution of massless bodies—which correspond to asteroids—perturbed by a planet in a circular or eccentric orbit using a fourth-order Hermite integration scheme. The parameters and their ranges are the same as those used in [2]; asteroids are initially uniformly distributed on the a-e plane, where a and e are the semimajor axis and eccentricity of the massless bodies, respectively. The other angle variables are uniformly distributed between 0 and 2π. We count bodies as temporary captures if they satisfy two conditions: (1) they must stay within 3 r_H from the host planet longer than one orbital period of the planet and (2) the minimum distance from the host planet is less than 1 r_H. If a body collides with the host planet or the Sun, or has $e > 1$ at $r > 30$ AU, it is removed from the calculation. The duration of temporary capture is defined as the time between the two moments when a body enters/exits the Hill sphere. The type of temporary capture is defined by the position and velocity vectors at the moment when the body enters the Hill sphere; via L_1 or L_2, and prograde or retrograde.

3. Results and Discussion

Figure 1 shows the cumulative distributions of temporary capture time of particles by a Martian mass planet with eccentricity = 0.02. For short-time temporary capture, the number of retrograde captures is more than that of the prograde captures. However, for long-time temporary capture longer than ~10 T_K (T_K is the orbital period of the host planet), the slopes for the prograde captures become shallower and the numbers exceed those of the retrograde captures. These long tails seen in prograde long captures is consistent with Suetsugu et al.(2011)[3]. For Martian mass planet cases, no large differences are seen between the L_1 and L_2 captures. We find that the broken power law fits each distribution nicely. The parameters to characterize the distribution are functions of the type of capture, the incident velocity to the Hill sphere, and the mass and eccentricity of the host planet. The details of these parameters will be discussed on our poster.

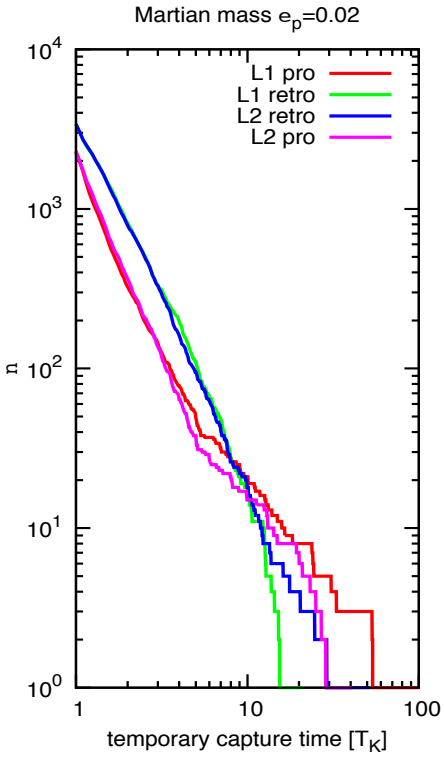

Figure 1: Cumulative number distribution of temporary capture time scaled by the orbital period of the host planet, a Martian mass planet with semimajor axis = 1.52 AU and eccentricity = 0.02. Each color indicates capture type; via L_1 or L_2, and prograde or retrograde.

Acknowledgements

This work was supported by JSPS KAKENHI grant Numbers 23740335 and 26800229. Data analyses were in part carried out on the PC cluster at the Center for Computational Astrophysics, NAOJ.

References

[1] Jewitt, D & Haghighipour, N., ARA&A, 45, 261, 2007.

[2] Higuchi, A. & Ida, S., AJ, 153, 4., 2017

[3] Suetsugu, R., Ohtsuki, K. & Tanigawa, T. (2011) AJ, 142, 6, 2011

EPSC Abstracts
Vol. 11, EPSC2017-499, 2017
European Planetary Science Congress 2017

ASTEROID MASS ESTIMATION WITH MARKOV-CHAIN MONTE CARLO

L. Siltala and M. Granvik
Department of Physics, P.O. Box 64, 00014 University of Helsinki, Finland (lauri.siltala@helsinki.fi)

Abstract

1. Introduction

Estimates for asteroid masses are based on their gravitational perturbations on the orbits of other objects such as Mars, spacecraft, or other asteroids and/or their satellites. In the case of asteroid-asteroid perturbations, this leads to a 13-dimensional inverse problem at minimum where the aim is to derive the mass of the perturbing asteroid and six orbital elements for both the perturbing asteroid and the test asteroid by fitting their trajectories to their observed positions. The fitting is typically carried out with linearized methods, in particular the least-squares method. These methods need to make certain assumptions regarding the shape of the probability distributions of the model parameters to describe the parameters' uncertainties. This is problematic as these assumptions have not been validated and, in fact, are known to be misleading [2].

2. Algorithm

We have developed a new Markov-chain Monte Carlo-based algorithm for mass estimation [5, 6, 7] using asteroid-asteroid perturbations. We use the Adaptive Metropolis scheme [4] which constantly updates the used covariance matrices based on the chain itself in order to ensure suitable shapes for the proposal distributions. This algorithm is implemented into a fork of the OpenOrb asteroid-orbit-computation software [3]. We now extend the algorithm to use multiple massless test asteroids simultaneously. We also include a proper observational error model [1] in our calculations.

3. Results

We present results computed with our algorithms and compare them to published results for our chosen asteroids. Our results agree with the published nominal mass estimates, but suggest that the published uncertainties may be misleading as a consequence of using linearized mass-estimation methods. Fig. 1 shows example results for asteroid (19) Fortuna in the form of weighted histograms of all accepted masses in the chain for two separate runs with different test asteroids. This clearly showcases the systematic effect that the choice of test asteroid can have on the results: as the perturber is the same in both cases, it naturally follows that the correct mass is also the same. In practice, however, we get very different results with different test asteroids, though the correct mass remains within the uncertainties of both distributions. If both test asteroids were used at the same time, one would expect that the resulting distribution would be similar to the overlapping area of the two separate histograms, as the perturber mass would have to fit both objects at once.

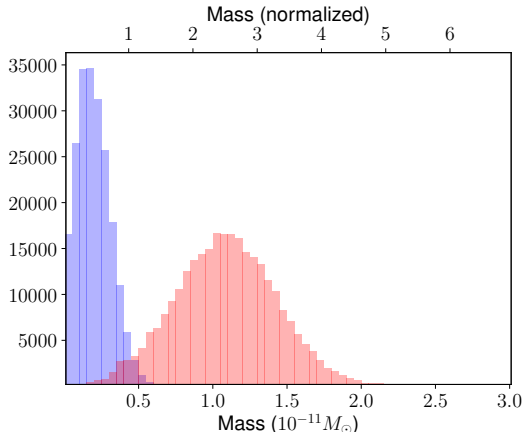

Figure 1: Results of the MCMC algorithm applied to asteroid pairs 19-3486 (blue) and 19-27799 (red). The lower x-axis represents mass in solar masses while the upper x-axis is normalized such that unity equals the weighted average of published values [2].

4. Summary and Conclusions

We have developed a new MCMC-based asteroid mass estimation algorithm, which gives results in line with previous literature values and suggests that uncertainties of prior estimates may be misleading as a conse-

quence of using linearized methods. Future work includes further improvements to our algorithm (such as automated outlier rejection and accounting for systematic offsets in the astrometry) as well as application to Gaia Data Release 2 data to be released in April 2018.

Acknowledgments

This work was supported by grants #299543 and #307157 from the Academy of Finland.

References

[1] Baer, J., Chesley, S. and Milani, A.: Development of an observational error model, Icarus, Vol. 212, pp. 438-447, 2011.

[2] Carry, B.: Density of asteroids, Planetary and Space Science, Vol. 73, pp. 98-118, 2012.

[3] Granvik, M., Virtanen, J., Oszkiewicz, D. and Muinonen, K.: OpenOrb: Open-source asteroid orbit computation software including statistical ranging, Meteoritics and Planetary Science, Vol. 44, pp. 1853-1861, 2009.

[4] Haario, H., Saksman, E., and Tamminen, J.: An adaptive Metropolis algorithm, Bernoulli, Vol. 7, pp. 223-242, 2002.

[5] Siltala, L. and Granvik, M.: Asteroid mass estimation using Markov-Chain Monte Carlo techniques, AAS/Division for Planetary Sciences Meeting Abstracts, 48, p. 324.01, Pasadena, USA, 2016.

[6] Siltala, L. and Granvik, M.: Asteroid mass estimation with Markov-chain Monte Carlo, Asteroids, Comets, Meteors Abstracts, Parallel6.b.2, Montevideo, Uruguay, 2017.

[7] Siltala, L. and Granvik, M.: Asteroid mass estimation using Markov-chain Monte Carlo, Icarus, submitted, 2017.

EPSC Abstracts
Vol. 11, EPSC2017-528, 2017
European Planetary Science Congress 2017

Studying the influence of target and projectile properties on low-velocity collisions

Gautier Nguyen[1], Naomi Murdoch[1], Alexis Calandry[1], Olivier Cherrier[1], Yves Gourinat[1]

[1]Institut Supérieur de l'Aéronautique et de l'Espace (ISAE-SUPAERO), Université de Toulouse, 31055 Toulouse, France

Abstract

To improve our understanding of landing on small bodies and of asteroid evolution, we have performed new experiments of low-velocity impacts into granular material in both normal and reduced-gravity. We study the influence of the target material, the projectile shape and orientation, and the gravitational acceleration.

1. Introduction

The number of small-body missions involving surface interactions has flourished in recent years. From the recent Rosetta and Hayabusa missions, to the current and future missions such as Hayabusa 2, OSIRIS-REx and AIDA. Given the small escape velocities of these missions' targets, the impact velocities of the landers are likely to be small (10s of cm/s or lower) in order to minimize the risk of rebounding into space. The understanding of low-velocity impacts is, therefore, important for missions involving surface interactions and will influence the lander deployment strategy, the mission design and operations, and even the choice of payload for the future missions. In addition to being of high importance for future space missions, the physics of low-velocity collisions in low-gravity, and the mechanical properties of small bodies and regolith, also have consequences for our understanding of planetary accretion processes, planetary ring dynamics, cratering processes and asteroid geophysical evolution.
Previous analysis of the results of the Rosetta *Philae* landing indicated the possibility of studying the surface mechanical properties from the landing data. Indeed, using the crater depth and rebound dynamics Biele et al. (2015) [1], estimated the compressive strength of the two landing sites of Philae to be ~1 kPa, and at least 2 MPa, respectively. However, the difficulties faced by this mission highlighted the complexities of small-body landing, and also our lack of knowledge on the physical properties of the regolith that composes the surface of these bodies.

2. Low-velocity collisions into granular material

Given that asteroids are covered with substantial regolith [2], the landing can be seen as a low-velocity and shallow impact onto a granular material, with velocities in the order of cm/s to 10's cm/s. Impacting a projectile into a granular layer has become a classical problem in granular physics studied from theoretical, numerical and experimental points of view.
Our previous low-gravity experimental results of impacts of a spherical projectile into quartz sand [3] indicate that the transition from the quasi-static regime to the inertial regime occurs for impact energies two orders of magnitude smaller than in similar impact experiments under terrestrial gravity. The lower energy regime change may support the notion that the quasi-static regime reduces as the effective gravity becomes lower, but may also be due to the increased hydrodynamic drag of the target material in our initial experiments.
Starting from the previous experimental works on this problem, we intend to study the influence of the target material in low-velocity collisions in order to identify the reason for the observed regime change. We will also verify and further the previously evidenced scaling laws [e.g., 4-6] by including the influence of the target material type, the projectile shape and orientation. Finally, we will also study the influence of varying the gravitational acceleration.

3. New Experimental trials

To further our previous experimental findings [3] we have performed a new campaign of experiments in both normal and reduced-gravity. In these trials, two different projectile shapes are considered: spherical (10 cm diameter) and cubic (10 cm wide). See Fig. 1. Both are metallic (fabricated out of 2017 aluminum alloy) and weigh ~1 kg. The cubic projectile can be oriented to initially impact the material on one of its sides, one of its corner or one of its faces which allow us to observe the importance of the impact

Figure 1: The two projectiles used in the experiment. Left: spherical projectile in an experiment with quartz sand. Middle: cubic projectile positioned to impact the quartz sand on the projectile edge. Right: cubic projectile positioned to impact the basalt gravel on the projectile corner.

orientation on the collision dynamics. Two inertial measurement units consisting of three-axis accelerometers and gyroscopes are contained within the projectile. Diverse target materials are tested in order to study the link between the collision dynamics and the mechanical properties of the material. The materials used are quartz sand (1-2.5 mm), basalt gravel (6 – 14 mm), three different sizes of soda lime glass beads (1.5, 5 and 10 mm) and, finally, polystyrene beads (2.5 mm).

3.1 Static trials

In the static case (1*g* gravitational acceleration), the target material is contained in a container dimensioned to avoid any boundary-effects during the low-velocity impact. The projectile drop-height (and consequently the impact velocity) is controlled by an adjustable rod to which the projectile is attached (and released from) using an electromagnet. To make the experiments as reproducible as possible, the target material is removed and then poured back into the container before each trial, to get rid of any prestrain effects. From the accelerometer data we can obtain the values of the collision duration, penetration depth and acceleration peak at various impact speeds and for different target materials.

3.2 Reduced-gravity trials

Experiments have also been performed in reduced-gravity (~ 0.02 – 0.1*g* effective gravitational acceleration) using our novel drop-tower facility [7]. The drop tower uses a system of counterweights and pulleys to adjust the acceleration of the surface container and consequently to simulate a reduced gravitational acceleration (Fig. 2). These experiments will allow us to study how the collision characteristics change with varying gravitation acceleration.

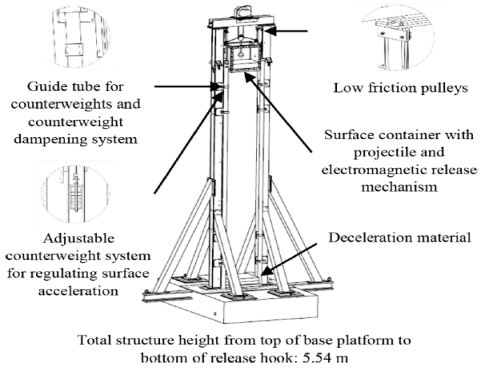

Figure 2: Isometric line drawing of the experiment and existing drop tower structure from [7]

4. Results

We will present our findings for the trials performed under both terrestrial and reduced-gravity conditions. Specifically, we will show how the collision dynamics (duration, peak accelerations, penetration depth) are influenced by the different target materials and the projectile shape for varying impact velocities.

Acknowledgements

This project benefited from financial support from CNES and from ESA. We thank Daniel Gagneux and Thierry Faure, for their help in designing and building the drop tower experiment.

References

[1] Biele et al., Science, 2015; [2] Murdoch et al., Asteroids IV, 2015. [3] Murdoch et al., MNRAS, 2017; [4] Katsuragi, Physics of Soft Impact and Cratering, 2016; [5] Goldman et al., PRE, 2008; [6] Tiwari et al., PRE, 2014 [7] Sunday et al., Rev. Sci. Inst., 2016

EPSC Abstracts
Vol. 11, EPSC2017-701-2, 2017
European Planetary Science Congress 2017

Spectral analyses of asteroids' linear features

A. Longobardo (1), E. Palomba (1,2), J.E.C. Scully (3), M.C. De Sanctis (1), F. Capaccioni (1), F. Tosi (1), A. Zinzi (2,4), A. Galiano (1), E. Ammannito (5), G. Filacchione (1), F.G. Carrozzo (1), M. Ciarniello (1), A. Raponi (1), F. Zambon (1), M.T. Capria (1,2), S. Erard (6), D. Bockelee-Morvan (6), C. Leyrat (6), F. Dirri (1), L. Nardi (1), C.A. Raymond (7)
(1) INAF-IAPS, via Fosso del Cavaliere 100, 00133 Rome, Italy (andrea.longobardo@iaps.inaf.it); (2) ASI-ASDC, Rome, Italy; (3) UCLA, Losa Angeles, CA, USA; (4) INAF-OAR, Rome, Italy; (5) ASI-URS, Rome, Italy; (6) LESIA, Observatoire de Paris/CNRS/UPMC/Université Paris-Diderot, Meudon, France, (7) JPL-Cal.Tech., Pasadena, California, USA

Abstract

Linear features are commonly found on small bodies and can have a geomorphic or tectonic origin. Generally, these features are studied by means of morphological analyses. Here we propose a spectroscopic analyses of linear features of different asteroids visited by space missions, in order to search for correspondence between spectral properties and origin of linear features.

1. Introduction

Four basic types of linear features have been identified on small bodies: grooves, troughs, ridges and modifications of crater shapes [1]. In turn, grooves can be divided in two types, basing on their origin: tectonic grooves are generated by subtle topographic changes or by fractures (filled by down-draining regolith), whereas geomorphic grooves are due to ejecta deposited on the surface.
In this work we analyse spectral properties of asteroids' linear features and search for a possible link with their origin.

2. Data

We study spectral data from the following asteroids: Eros, Lutetia, Vesta and Ceres. Eros has been observed by the NIS spectrometer (on board the NASA NEAR mission), covering the spectral range 0.8-2.5 μm [2]. Lutetia has been observed during the ESA/Rosetta flyby from the VIRTIS-M imaging spectrometer [3], whereas Vesta and Ceres have been the target of the Dawn mission and were extensively observed from the VIR mapping spectrometer [4]. VIRTIS-M and VIR are very similar instruments, composed of an optical head, composed of a visible (0.2-1 μm) and an infrared (1-5 μm) channel and having imaging properties.

We considered also NIRS data (JAXA/Hayabusa mission) from Itokawa [5], but currently no linear features have been detected on this asteroid.

3. Preliminary results

3.1 Eros

The Eros surface is dominated by tectonic grooves [6]. The MSI camera data did not show albedo variations in correspondence of grooves, with the exception of features near the Selene crater which show an albedo decrease [7]. Analysis of NIS data will allow identifying possible variations of pyroxene band depths (centered at 1 and 2 μm, respectively).

3.2 Lutetia

Lutetia is also dominated by tectonic grooves, in some cases associated to albedo variations [8]. VIRTIS data identified albedo increase in correspondence only of one groove (Figure 1) [9]. However, due to its radial orientation, we cannot discard that this groove has a geomorphic origin.

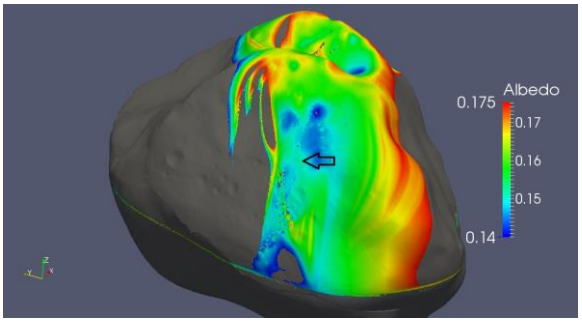

Figure 1. Albedo map of Lutetia [9]. The arrow indicates the groove.

3.3 Vesta

Vesta shows different types of linear features on its surface, i.e. graben (a particular type of trough) [10], geomorphic grooves, tectonic grooves and ridges. Graben are never associated to albedo or spectral changes. The same is true for tectonic grooves, even if in this case some exceptions occur (i.e. darkening) [9]. On the other side, geomorphic grooves are always associated with albedo decrease (Figure 2), indicating a different composition (since grain size is thought to be constant [10]). Finally, the peculiarity of ridges is the color, often bluer (i.e. lower spectral slope) than surroundings, probably indicator of a younger age.

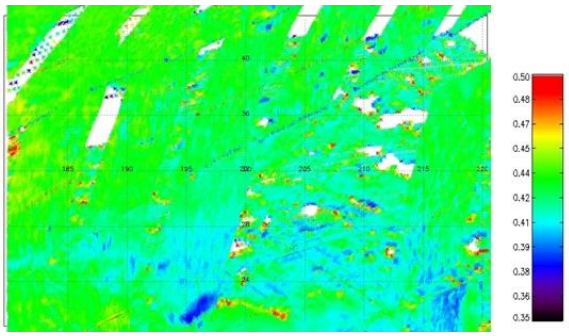

Figure 2. Albedo map of a Vesta region [9]. The bluer markings (i.e. lower albedo) correspond to geomorphic grooves.

3.4 Ceres

Ceres shows linear features of different origin. Their spectral analysis is in progress and is based on absorption bands at 2.7 μm and 3.1 μm, due to hydrated and ammoniated materials, respectively [11], as well as to visible and infrared albedo.

4. Conclusions

The analysis performed so far identifies that linear features of structural origin (tectonic grooves and troughs) are generally not associated to spectral variations. However, some exceptions occur and concern fractures, probably because of exposition of subsurface, which can have a different composition with respect to the surface.
On the other hand, geomorphic grooves and ridges can be discriminated on spectral maps, due to their different albedo, colour or depth of absorption bands. This indicates that this type of feature is generally composed by a material different than surroundings, and the difference can concern composition, physical properties or age.
Further spectral analyses are in progress to confirm these results.

Acknowledgements

VIR and VIRTIS are funded by the Italian Space Agency (ASI) is managed by INAF-IAPS, Rome-Italy. VIR was built by Selex-Galileo, Florence-Italy. VIRTIS was built by a consortium formed by Italy, France and Germany. The VIRTIS consortium includes also LESIA (France) and DLR (Germany).

References

[1] Thomas, P.C. and Prockter, L.M. (2010), In: Watters, T.R., Schultz, R.A. (Eds.), Planetary Tectonics. Cambridge, University Press.

[2] Robinson, M. et al. (1995), Meteoritics 30, 5, 566

[3] Coradini, A. et al. (2007), SSR 128, 529-559.

[4] De Sanctis, M.C. et al. (2011), SSR 163, 329-369

[5] Abe, M. et al. (2006), Science 312, 1334-1338

[6] Prockter, L. et al. (2002), Icarus 155, 75-93

[7] Veverka, J. et al. (1997), JGR 102, 23709-23728

[8] Thomas, N. et al. (2012), PSS 66, 96-124

[9] Longobardo, A. et al. (2015), Icarus 259, 72-90

[10] Palomba, E. et al. (2014), Icarus 240, 58.72

[11] De Sanctis, M.C. et al. (2015), Nature, doi:10.1038/nature16172

EPSC Abstracts
Vol. 11, EPSC2017-732, 2017
European Planetary Science Congress 2017

Impact of asteroïdal hydrothermal alteration on organics

V. Vinogradoff (1), S. Bernard (1), C. Le Guillou (2), M. Jaber (3) and L. Remusat (1)
(1) IMPMC, UMR CNRS 7590, Sorbonne Universités, MNHN, UPMC, IRD UMR 206, Paris, France, (2) UMET – UMR-CNRS 8207, Université Lille 1, (3) LAMS, UMR CNRS 8220, UPMC, Paris, France. (vassilissa.vinogradoff@mnhn.fr)

Abstract

Unravelling the evolution of simple organic molecules trapped in ices after they were accreted into asteroids requires better constraining how they would be modified by hydrothermal alteration, which happened in carbonaceous chondrites (CC) [1]. We have experimentally investigated the chemical evolution of interstellar organic molecule submitted to hydrothermal conditions mimicking asteroidal alteration. In particular, we investigated the role of phyllosilicates in the preservation/degradation of organic matter. We observed that a simple organic molecule (HMT) undergo complex chemical transformation during hydrothermal alteration, with the formation of an insoluble organic matter. Phyllosilicates have influenced the chemical reactions by concentrating a significant fraction of the newly formed organics.

1. Introduction

The origin and evolution of the suite of organic compounds found in chondrites remain complex to disentangle. Whereas they are somehow inherited from the interstellar medium (ISM), further evolutions in the protosolar disk [2] as well as in the parent body [1] have contributed to their present molecular composition. The dust in the ISM is composed of a mixture of organic compounds and/or silicates trapped within ices (<20 K). Irradiation experiments (UV and cosmic rays) performed on ices analogues (from 10 K to 300 K) reproduce many of the molecules observed in the ISM. Annealed above 300 K, these experiments yield an organic-rich residue dominated by hexamethylenetetramine (HMT, $C_6H_{12}N_4$) [3-4]. The parent asteroids of carbonaceous chondrites (CC) have all experienced hydrothermal alteration of variable intensities which has affected the organic matter (OM) [5]. However, the extent of the modification induced by alteration remains unknown and prevents elucidating the question of their pre-accretion history.

2. Hydrothermal experiments

Hydrothermal experiments were conducted at 150 °C in Teflon bombs closed in a N_2 atmosphere, for durations up to 31 days. The water pH was set to 10 using KOH. In a first set of experiments, HMT (0.7 M) was submitted to alteration. In a second set, 100 mg of synthetic (organic-free) clays was added (either a Na-montmorillonite or a Fe^{3+}-nontronite) to investigate the role of the clay mineral structure and composition. Reaction products were characterized by gas-chromatography coupled to mass spectrometry (GC-MS), Infrared spectroscopy (IR), synchrotron-based X-ray absorption near edge structure (XANES) spectroscopy, X-ray diffraction (XRD) and thermogravimetry (TGA).

In the absence of clays, HMT is rapidly decomposed and both soluble and insoluble OM are formed. Most of the reaction occurs in the first 20 days (Fig. 1). After 7 days, a suite of soluble, aromatic nitrogen-bearing molecules and amides, compounds is formed (around 150 species with m/z of 59 to 254 - 31 days experiment).

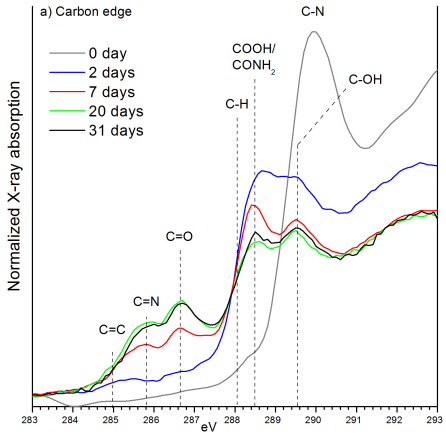

Figure 1: Carbon K-edge XANES spectra of the liquid reaction products of HMT 0.7 M after 0, 2, 7, 20, 31 days. Increase of aromatic, amine and carbonyl functions is observed.

A complex, insoluble N-rich organic compound (< 1 wt.%) is formed after 7 days. Its chemical signature, measured by XANES and IR (Fig. 2), reveals aromatic, carbonyl, amide and carboxylic functions. Its elemental composition is H/C=1.2, N/C=0.26 and O/C=0.31.

In the presence of clays, after 31 days, the number of soluble organic products is reduced; only 36 and 66 species (mainly between m/z 73 to 124, with some higher molecular weight moieties: up to 254 m/z) are observed from HMT + nontronite and HMT + montmorillonite mixtures, respectively. XRD analysis of the solid residues show an increase of the interlayer spacing, which suggests that organic matter has been inserted within the phyllosilicate interlayers. The solid residue displays infrared features of organic compounds (31 days; Fig. 2). The absorption bands due to OM depend on the nature of the clay. TGA reveals that the sample with nontronite contains up to 6.5 wt.% of organic matter and the sample with montmorillonite up to 8 wt.%, both after 31 days.

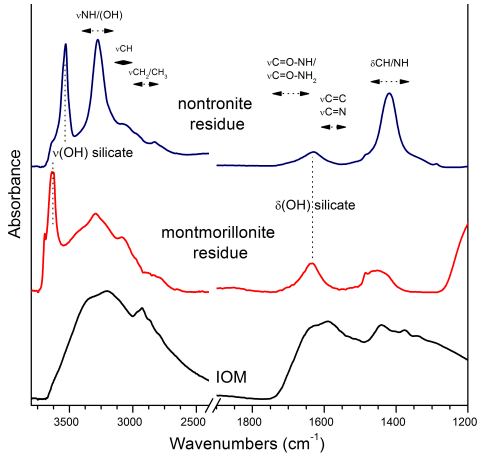

Figure 2: Infrared spectra of the clay products after 31 day long of hydrothermal alteration experiments with HMT, compared to the IOM spectrum at 31 days from HMT alone.

3. Discussion and conclusions

Our study reveals that, under hydrothermal conditions, a simple interstellar organic molecule such as HMT is, in a few days, decomposed into a suite of diverse molecular weight soluble compounds and a insoluble N-rich OM. The reaction mechanism starts by the decomposition of HMT into formaldehyde and ammonia. Then, the general evolution of the OM resembles the Maillard reaction, a complex set of reaction which involve amines and sugars through polymerization/condensation and ultimately the formation of an IOM. If HMT, formaldehyde or ammonia are among the molecules accreted in parent bodies, the above described reaction pathways would have occurred and would constitute an alternative route to form IOM in CC.

The addition of clays in the system drastically modifies the reaction products. The reduced diversity of soluble species could be due to the absorption of their precursors on the clay surfaces or their insertion within the interlayer spaces, which would have prevented them of further reactions.

This may have important implications for the study of chondrites. First, if soluble molecules were absorbed/enclosed, they would not be release by solvent extraction and would constitute a "hidden" OM reservoir, not yet fully investigated. Second, phyllosilicates have heterogeneous compositions and structures both within one given chondrite and in different chondrite groups. Therefore, if different reaction pathways are involved when different clays are present, it could, at least in part, explain the heterogeneity and diversity of OM in chondrites. Finally, the evolution of the OM enclosed in phyllosilicates could be different from the "free" one, which would also lead to different reactivity and transformation behaviour.

Altogether, this study constitutes a step forward to link the molecules observed in the ISM with the molecules observed in CC. The formation of insoluble OM from HMT at low temperature is demonstrated, and we suggest that the importance of the interactions with phyllosilicates may have been so far overlooked and should now be studied in more details in order to fully understand the evolution of organic matter during hydrothermal alteration.

Acknowledgements

This work is funded by the city of Paris (program "Emergence"), and the National Museum of Natural History in Paris through the ATM funding resources. We are grateful to Christelle Anquetil for GC-MS, Matthieu Lebon and Xavier for IR spectroscopy and Ludovic Delbes for XRD analysis.

References

[1] Remusat L. (2015), *EMU notes in Mineralogy*, *15*, chapter 8. [2] Herbst et van Dishoeck, (2009) *Annu. Rev. Astro. Astrophys* [3] Munoz-Caro G.M., Schutte W.A. (2003) *A&A*, *412*, 121. [4] Vinogradoff V., Rimola A., Duvernay F., Danger G., Theulé P., Chiavassa T. (2012), *PCCP*, *14*:12309. [5] Alexander et al. (2007), GCA, 71, 4380-4403, [6] Le Guillou et al. (2014) *GCA*, *131*, 368-392.

EPSC Abstracts
Vol. 11, EPSC2017-745-1, 2017
European Planetary Science Congress 2017

Exogenous material on asteroids: hydration on (16) Psyche.

C. Avdellidou[1] and M. Delbo'[2]
1 Scientific Support Office, Directorate of Science, European Space Research and Technology Centre (ESA/ESTEC), 2201 AZ Noordwijk, The Netherlands (chrysa.avdellidou@esa.int)
2 Observatoire de la Cote d'Azur, Boulevard de l'Observatoire-CS34229, 06304 Nice cedex 4, France

Abstract

Here we present the results of the modelling on asteroid Psyche, in order to interpret the detection of the hydration band on its surface. We focus on the scenario that the hydration is exogenous and was delivered by low and high velocity impacts from bodies of the central and outer main asteroid belt. We propose the source regions of impactors, calcuate the number of collisions and estimate the final implanted mass on Psyche.

1. Surface contamination

The contamination of asteroid surfaces via impacts is a mechanism that has been proposed first time for the asteroid (4) Vesta after the observations of the dark material [1]. This was later verified by theoretical models of contamination [2, 3] and also by laboratory experiments [4, 5] that demontrated the survival of the impactor and the deposition of material at higher than previously thought speeds. However, this amount of mass is strongly related to the impact speed in addition to the target material and porosity.

2. (16) Psyche

In this work we are focused on the asteroid Psyche, the target of the NASA's space mission. Psyche is an outer Main Belt asteroid which vextremely high radar albedo indicates a metallic compasition. Although independent studies agree for the asteroid's size to be D=226 km/s [6], the mass is still not well etsimated and thus the bulk density of the body flactuates between 3.7 and 4.5 g/cc [6, 7]. Considering the extreme density and the high radar albedo the asteroid could be a stony/iron body with no macroporosity or an iron/nickel body with quite high macroporosity of 40%.
Recent spectroscopic observations identified the 3 μm feature that is related to the hydration of the surface [8]. The band was observed in four different phases and shows a small variation on the type of hydration and band-depth. The presense of hydration sets new constrains on the study of the asteroid. If Psyche is an iron core of a differentiated body, then any hydration cannot have be endogenous but must have been deposited to the surface by another process.

3. Our model

Following the hypothesis of the exogenous origin of the hydration on Psyche, the questions that arise now are:

- which bodies can provide this exogenous material?
- how much material can these impactors deliver?
- is this material enough to be spectroscopically detected?

The investigation is done in three steps. First of all we have identified the area around the target that can provide impactors at speeds taken from the laboratory experimets. In this area we hunted for the hydrated sources of the potential impactors. Next we computed the number of collisional events and the mass that was finally implanted on the surface of Psyche.

4. Implications

The implications from this work is multi-dimensional. If the amount of the hydrated implanted material is not sufficient for ground-based telescopic detection, then we need to identify more hydrated sources in the area of Psyche. This means that hydration is more abundant and thus more spectroscopic observations are needed for the asteroids of the central and outer belt in order to hunt for the 3 μm feature. In this case a better constrain of the bulk density could couple the excess of the hydrated material and indicate a possible endogenous origin. On the other hand, the calculated mass

can be more than the expected from the observations. Here we should note that each impact deposits material but also removes or hides the pre-existing one. This is not well quantified and any impactor carrying non-hydrated material can obscure previous depositions, so any discrapancy in mass can be due to impact gardening. In any case we can be more and more confident with the idea of the impact implantation of exogenous material on asteroid surfaces. Observations start to reveal spectral features on bodies that cannot match with the bulk composition. In case of Psyche, the NASA's space mission will provide a clear image when will reach the puzzling asteroid. Using this work we can have a first prediction for asteroi-targets of other missions, such as NASA's OSIRIS-REx that will start mapping the surface of the near Earth Asteroid Bennu in 2018-2019.

References

[1] Reddy, V. et al.: Delivery of dark material to Vesta via carbonaceous chondritic impacts, Icarus, Volume 221, Issue 2, p. 544-559, 2012.

[2] Turrini, D. et al.: The contamination of the surface of Vesta by impacts and the delivery of the dark material, Icarus, Volume 240, p. 86-102, 2014.

[3] Turrini, D. et al.: Olivine on Vesta as exogenous contaminants brought by impacts: Constraints from modeling Vesta's collisional history and from impact simulations, Icarus, Volume 280, p. 328-339, 2016.

[4] Avdellidou, C. et al.: Survival of the impactor during hypervelocity collisions - I. An analogue for low porosity targets, Monthly Notices of the Royal Astronomical Society, Volume 456, Issue 3, p.2957-2965, 2016.

[5] Avdellidou, C. et al.: Survival of the impactor during hypervelocity collisions - I. An analogue for high porosity targets, Monthly Notices of the Royal Astronomical Society, Volume 464, Issue 1, p.734-738, 2017.

[6] Shepard, M. et al.: Radar observations and shape model of asteroid 16 Psyche, Icarus, Volume 281, p. 388-403, 2017.

[7] Hanus, J. et al.: Volumes and bulk densities of forty asteroids from ADAM shape modeling, Astronomy and Astrophysics, 2017.

[8] Takir, D. et al.: Detection of Water and/or Hydroxyl on Asteroid (16) Psyche, The Astronomical Journal, Volume 153, Issue 1, article id. 31, 6 pp., 2017.

EPSC Abstracts
Vol. 11, EPSC2017-750, 2017
European Planetary Science Congress 2017

Near-surface bulk densities of asteroids derived from dual-polarization radar observations

A. K. Virkki (1), P. A. Taylor (1), L. F. Zambrano-Marin (1,2), E. S. Howell, (3), C. Lejoly (3), M. C. Nolan (3), E. G. Rivera-Valentin (1), B. A. Aponte (1)

(1) Arecibo Observatory, Puerto Rico, USA, (2) Escuela Internacional de Posgrado, University of Granada, Spain, (3) Lunar and Planetary Laboratory, University of Arizona, Arizona, USA (avirkki@naic.edu / Fax: +1-787-878-1861)

Abstract

We present a new method to constrain the near-surface bulk density and surface roughness of regolith on asteroid surfaces using planetary radar measurements. The number of radar observations has increased radically during the last five years, allowing us to compare and contrast the radar scattering properties of different small-body populations and compositional types. This provides us with new opportunities to investigate their near-surface physical properties such as the chemical composition, bulk density, porosity, or the structural roughness in the scale of centimeters to meters.

1. Introduction

The dual-polarization radar observations are a powerful, cost-effective tool to characterize both the dynamical and the physical properties of the terrestrial planets, moons, and the small bodies of the Solar System. The number of radar-observed asteroids and comets has increased rapidly over the last five years enabling improvements in statistical analysis. Also, the laboratory studies of the materials that are relevant to asteroids and comets have improved during the last decade (e.g., [2, 3]).

Our goal is to improve the theoretical methodology for deriving the near-surface densities of asteroids, which has been formerly challenging due to a small number of radar-observed targets.

2. Methods

In a typical planetary radar measurement a circularly polarized signal is transmitted using either a frequency of 2380 MHz (wavelength of 12.6 cm) or 8560 MHz (3.5 cm). The echo is received simultaneously in the same circular (SC) handedness and the opposite circular (OC) handedness as compared to the transmitted signal. The delay and doppler frequency of the signal give highly accurate astrometric information, and the intensity and the polarization are suggestive of the physical properties of the target's near-surface.

The penetration depth of the signal is typically a few wavelengths depending on the absorption of the material. If the surface is smooth and the effective near-surface is homogeneous in the wavelength-scale, the echo is received fully in the OC polarization. Wavelength-scale surface roughness or boulders within the effective near-surface volume increase the fraction of echo power received in the SC polarization [4, 7].

The radar reflectivity of the target can be described using the radar albedo, $\hat{\sigma}$. For an ideal metallic sphere, $\hat{\sigma} = 1$.

The OC-polarized part of the echo is composed of a quasi-specular component and a diffuse component. Traditionally, the OC radar albedo has been treated as a product of the Fresnel reflection coefficient (at normal incidence), R_F, and the backscatter gain factor, g: $\hat{\sigma}_{OC} = gR_F$ [5]. For an ideal sphere, $g = 1$. However, there has been a lack of methods to determine R_F or g independently. Instead, g is often simply guessed to be in the range of 1.1-1.5.

To resolve this problem, we utilize the information that the diffuse components of the OC and SC parts are correlated (Fig. 1). A linear least-squares fit to the detected values of $\hat{\sigma}_{OC}$ and $\hat{\sigma}_{SC}$ allows us to separate the diffuse-scattering part from the quasi-specular part of $\hat{\sigma}_{OC}$. Thus we are able to evaluate the surface roughness of a specific target compared to other similar objects and also approximate the bulk electric permittivity (or the refractive index, m) of only the regolith that is composed of grains much smaller than the wavelength. For the latter part, we can use the following relation [1]:

$$\hat{\sigma} = R_F = \left| \frac{m-1}{m+1} \right|^2 \quad (1)$$

Combined with the spectro-photometric informa-

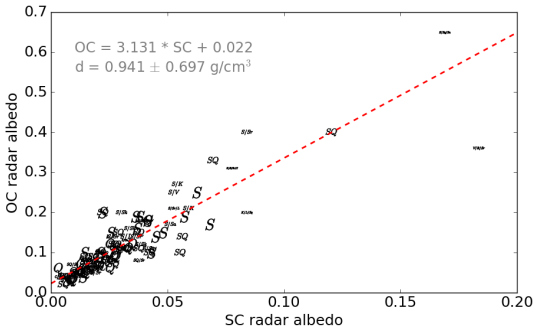

Figure 1: The diffuse parts of the OC and SC polarized echoes are correlated so that for asteroids that have a similar chemical composition, such as the S- and Q-type asteroids, the SC and OC radar albedos can be found to follow a certain trend. When $\hat{\sigma}_{SC} = 0$, $\hat{\sigma}_{OC} \approx R_F$. The $\hat{\sigma}_{OC}$-axis intercept point as well as the gradient of the line depend on the electric permittivity of the targets.

tion of the target and laboratory studies of the permittivity-density dependence provides us a way to set strong constraints on the density or porosity of the target's near-surface.

Sources of errors for the method are caused by the size estimation of the target, which is required for assessing the radar albedos. In addition, part of the echo is scattered by an inclined surface, which sets a requirement for a correcting factor. The radar reflectivity as a function of the scattering angle has been shown for the lunar surface by, e.g., Thompson et al. [6].

3. Summary and Conclusions

We improve the methods to interpret the physical properties of planetary surfaces using radar observations. In this paper, we concentrate on asteroids. The new method allows us to obtain strong evidence on the electric permittivity of small bodies of similar chemical compositions. Furthermore, we can estimate the density or the porosity of the material by utilizing laboratory measurements of the relation of the electric permittivity to these parameters. This provides us an access to information on the near-surface physical properties such as the abundance of metal, bulk density, or the structural roughness in the wavelength scale. A major part of this information, which is essential for landing space probes and understanding how these bodies were formed, is not accessible with other ground-based methods.

Acknowledgements

The Arecibo Planetary Radar Program is fully supported by NASA's Near-Earth Object Observations Program through grants no. NNX12AF24G and NNX13AF46G awarded to Universities Space Research Association (USRA). The Arecibo Observatory is an NSF facility operated under cooperative agreement by SRI International, USRA, and UMET.

References

[1] Bohren, C. F., and Huffman, D. R.: Absorption and Scattering of Light by Small Particles. John Wiley & Sons, Inc., USA, 1983.

[2] Brouet, Y., Levasseur-Regourd, A. C., Sabouroux, P., Encrenaz, P., Thomas, N., Heggy, E., and Kofman, W.: Permittivity measurements of porous matter in support of investigations of the surface and interior of 67P/Churyumov-Gerasimenko, Astronomy & Astrophysics, 583, A39, 2015.

[3] Carley, R. A., and Heggy, E.: Finite difference time domain simulation of radar wave propagation through comet nuclei dielectric models, Meteoritics & Planetary Science, 43, 6, 1085-1095, 2008.

[4] Fa, W., Wieczorek, M. A., and Heggy, E.: Modeling polarimetric radar scattering from the lunar surface: Study on the effect of physical properties of the regolith layer, Journal of Geophysical Research, 116, E03005, 2011.

[5] Ostro, S. J., Campbell, D. B., and Shapiro, I. I.: Main-belt Asteroids: Dual-Polarization Radar Observations, Science, 229, 442-446, 1985.

[6] Thompson, T. W., Ustinov, E. A., and Heggy, E.: Modeling radar scattering from icy lunar regoliths at 13 cm and 4 cm wavelengths, Journal of Geophysical Research, 116, E01006, 2011.

[7] Virkki, A., and Muinonen, K.: Radar scattering by planetary surfaces modeled with laboratory-characterized particles, Icarus, 269, 38-49, 2016.

EPSC Abstracts
Vol. 11, EPSC2017-776, 2017
European Planetary Science Congress 2017

Range of phase integral values for asteroids

V. G. Shevchenko (1,2), and I. N. Belskaya (1)
(1) Astronomical Institute of V. N. Karazin Kharkiv National University, Kharkiv, Ukraine, (2) Department of Astronomy and Space Informatics of V. N. Karazin Kharkiv National University, Kharkiv, Ukraine, (shevchenko@astron.kharkov.ua / Fax: +38-057-7005349)

Abstract

The values of the phase integral were determined for the main asteroid composition types using brightness phase functions in the wide phase angle range from space mission data. We found that the range of phase integral values for asteroids of different composition is within 0.34-0.54 with an average value of 0.42.

1. Introduction

The phase integral q is a main component for determination of the Bond albedo that enters into the thermal equilibrium equation and used for analyzing data obtained in the infrared wavelength range. Different authors have obtained different estimations of the phase integral of asteroids. Morrison [1] used the value of phase integral q=0.6. Later the relationship between q and G parameter of the HG-function [2] was used in [3-5]. Similar relationship has been proposed between q and G_1, G_2 parameters of the HG_1G_2-function [6]. The estimations of phase integrals have been made for asteroids using numerical integration of the phase function of brightness from space mission data [7, 8]. Here we investigate how the phase integral depends on asteroid composition types.

2. Results

The detailed observations of phase function of asteroid brightness have revealed their similarity within the same compositional types [9]. Based on the average G, G_1 and G_2 parameters for the main compositional types and the proposed relations between q and these parameters, the phase integral q lies in the range from 0.34 (low-albedo asteroids) to 0.64 (high-albedo asteroids). For some asteroids the phase functions of brightness have been obtained in a wide region of phase angles which allow direct calculation of the phase integral. To obtain the phase function for the S-type we have combined the data for the asteroids 1862 Apollo and 5535 Annefrank [10, 11]. We have obtained the value of q equal to 0.44 by the numerical integration. Using the data for the C-type asteroid 253 Mathilda [8, 12] and for the E-type asteroid 2867 Steins [13] we obtained q equals to 0.34 and 0.54, respectively. Note, that the value of the phase integral q=0.26 of 253 Mathilda given in [8] is smaller compared to our determination. The published values of phase integrals q=0.40 for the MU-type asteroid 21 Lutetia [7] and q=0.44 for the V-type asteroid 4 Vesta [14] are close to the values for the S-type asteroids. These data show that the range of q for asteroids of different types is within 0.34-0.54. The range is smaller as compared to values calculated using the G or G_1 and G_2 parameters [15]. We used the composite phase function of brightness for these asteroids (Fig. 1) to determine an average value of the phase integral.

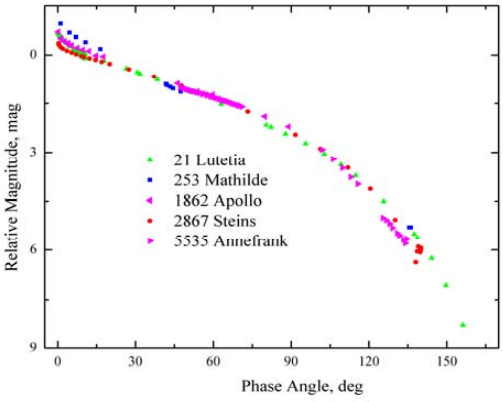

Figure 1: Composite magnitude phase function of asteroids [7, 8, 10-13].

There are differences in magnitude behavior at small and large phase angles, but these differences are

substantially less than global brightness changes in the range of phase angles of 0-180 deg. We have obtained the value of q=0.42 for the whole data set.

3. Conclusions

A range of the values of the phase integral for asteroids of different compositional types lies from 0.34 to 0.54 with an average value of q =0.42. These values can be used for determination of the Bond albedo of asteroids.

References

[1] Morrison, D.: Asteroid sizes and albedos. Icarus, Vol. 31, pp. 185–220. 1977.

[2] Bowell, E., Hapke, B., Domingue, D., et al.: Application of photometric models to asteroids. In Asteroids II. Tucson. Univ. Arizona Press. P. 524−556, 1989.

[3] Tedesco, E. F., Noah, P. V., Noah, M., Price, S. D.: The supplemental IRAS minor planets survey. Astron. J., Vol. 123, pp. 1056−1085, 2002.

[4] Masiero, J. R., Mainzer, A. K., Grav, T., et al.: Main belt asteroids with WISE/ NEOWISE. I. Preliminary albedos and diameters. Astrophys. J., Vol. 741, p. 68, 2011.

[5] Usui, F., Kuroda, D., Muller, T. G., et al.: Asteroid catalog using Akari: AKARI/IRC mid-infrared asteroid survey. Publ. Astron. Soc. Japan, Vol. 63, pp. 1117–1138, 2011.

[6] Muinonen, K., Belskaya, I. N., Cellino, A., et al.: A three-parameter phase-curve function for asteroids. Icarus, Vol. 209, pp. 542–555, 2010.

[7] Masoumzadeh, N., Boehnhardt, H., Li, J.-Y., et al.: Photometric analysis of Asteroid (21) Lutetia from Rosetta-OSIRIS images. Icarus, Vol. 257, pp. 239–250, 2015.

[8] Clark, B. E., Veverka, J., Helfenstein, P., et al.: NEAR photometry of asteroid 253 Mathilde. Icarus, Vol. 140, pp. 53−65, 1999.

[9] Belskaya, I. N., and Shevchenko, V. G.: Opposition effect of asteroids. Icarus, Vol. 146, pp. 490-499, 2000.

[10] Harris, A. W., Young, J. W., Goguen, J., et al.: Photoelectric lightcurves of the asteroid 1862 Apollo. Icarus, Vol. 70, pp. 246-256, 1987.

[11] Newburn, R. L., Duxbury, T. C., Hanner, M., et al.: Phase curve and albedo of asteroid 5535 Annefrank. J. Geophys. Res., Vol. 108, pp. 5117-5122, 2003.

[12] Mottola, S., Sears, W. D., Erikson, A., et al.: The slow rotation of 253 Mathilde. Planet. Space Sci., Vol. 43, pp. 1609-1613, 1995.

[13] A'Hearn, M. F., Feaga, L. M., Bertaux, J.-L., et al.: The far-ultraviolet albedo of Steins measured with Rosetta-ALICE. Planet. Space Sci., Vol. 58, pp. 1088−1096, 2010.

[14] Hicks, M. D., Buratti, B. J., Lawrence, K. J., et al.: Spectral diversity and photometric behavior of main-belt and near-Earth vestoids and (4) Vesta: A study in preparation for the Dawn encounter. Icarus, Vol. 235, pp. 60–74, 2014.

[15] Shevchenko, V. G., Belskaya, I. N., Muinonen, K., et al.: Asteroid observations at low phase angles. IV. Average parameters for the new H, G_1, G_2 magnitude system. Planet. Space Sci., Vol. 123, pp. 101−116, 2016.

EPSC Abstracts
Vol. 11, EPSC2017-828, 2017
European Planetary Science Congress 2017

Spectroscopy and photometry of CAI-rich asteroids

P. Tanga (1), M. Devogele (1,2), Ph. Bendjoya (1), A. Cellino (3), J.Surdej (2)
(1) UCA, UNS, Observatoire de la Côte d'Azur, Laboratoire Lagrange UMR7293/CNRS, (2) Université de Liège, Technologies and Astrophysics Research (STAR) Institute, Liège, Belgium (3) INAF/Osservatorio Astrofisico di Torino, Torino, Italia

Abstract

Asteroids that are classified as L-type in the classification that includes the Near-Infrared, are known to be a peculiar category of objects. They are named "Barbarians" from the first discovered (234 Barbara) and exhibit an anomalous high percentage of Calcium-Aluminum-rich-Inclusions (CAIs), responsible of a spinel absorption feature in the near infrared (around 2.1-2.2 μm). They also seem to have unusually high rotation periods, and large amplitude light curves. We started a campaign of NIR spectroscopy, photometry and polarimetry to shed a light on such properties and found a large variety of CAI abundances.

1. Observational campaign

The goal of our campaign was to obtain a the most complete physical characterization possible, concerning rotation periods, shapes, new polarimetric measurements, visible and NIR spectroscopy.

Polarimetry is an essential aspect, as Barbarians have a strong polarization parallel to the scattering plane at small phase angles, and a transition to perpendicular polarization at unusually high phase angles. Results obtained on this specific aspect will be introduced by Cellino et al. in the special session "Interpretation of observational data using spectro-polarimetric techniques" of EPSC2017.

Here we will focus mostly on the results by the other techniques.

We were able to coordinate a network of 15 telescopes around the world, to perform asteroid photometry of 16 targets, obtaining (or refining) their rotation period and determining an overall shape. [1][2]

We also obtained visible and NIR spectra for 15 asteroids [3]. Archive data were exploited to complete our sample.

Some of the asteroids in our sample belong to the Klumpkea and the Watsonia families. Others, to the scattered Henan group, probably a scattered collisional family that cannot be found by traditional clustering techniques based on dynamical properties [4].

2. Main results

Our photometric campaign shows that the anomalous distribution of rotation period, favoring long periods, is confirmed. We searched for the evidence of a widespread presence of possible concavities, on the example of 234 Barbara [3] but our results are not conclusive in this respect.

The most original results is provided by combining polarimetry and composition, showing that (1) there is a large variety of CAI abundance in our sample of L-type asteroids, ranging from negligible, to anomalously high, and (2) that this abundance is correlated to the variation of polarization rate with phase angle.

We also find a consistent behavior of the polarization related to the change in refraction angle of the spinel contained in the CAIs. Our study thus finds a strict link between the presence of spinel and the polarimetric anomaly of L-types.

References

[1] Devogele et al. 2017, Shape and spin determination of Barbarian asteroids, A&A submitted

[2] Tanga et al. 2015, The non-convex shape of (234) Barbara, the first Barbarian, MNRAS 448-4, 3382

[3] Devogele et al. 2017, New polarimetric and spectroscopic evidence of anomalous enrichment in spinel-bearing Calcium-Aluminium-rich Inclusions among L-type asteroids, Icarus, submitted

[4] Milani, A., et al. 2014, Icarus, 46, 239

EPSC Abstracts
Vol. 11, EPSC2017-836, 2017
European Planetary Science Congress 2017

NEO Data Exchange and Collaboration Service – NEODECS

A. Kryszczyńska (1), T. Kwiatkowski (1), P. Bartczak (1), A. Adamczyk (2) and G. Taberski (2)
(1) Astronomical Observatory, A. Mickiewicz University, Poznań, Poland (agn@amu.edu.pl), (2) ITTI, Poznań, Poland

Abstract

We work on a new web service (NEODECS) for collecting and sharing data on Near Earth Objects and facilitating collaboration among observers and researchers. Instead of having to maintain the content ourselves, we will only provide a tool for astronomers to register their databases, broadcast observing plans, seek collaborators as well as offer free telescope time to others. NEODECS can be extended in the future to other Small Solar System Bodies.

1. Introduction

Every day NEO observations are performed in a number of observatories. Raw data collected during those activities are rarely available to the scientific community, and results obtained from their analysis are not always published (or published with significant delay, when a longer observing campaign is completed). Some data are placed in various databases and web sites with either an open access to the whole content or only to a summary of various data products in an archive. Current internet search engines are becoming more and more sophisticated but due to the exponential grow of information finding relevant data is not easy. E-mail is still a basic tool for collaboration among the observers but often requires additional web services to be used, and social media are only a partial solution as they are not optimized for astronomy.

2. Aims

The goal of the NEO Data Exchange and Collaboration Service (NEODECS) is to create an open access central repository of structured meta data on NEOs, as well as a platform for collaboration among NEO researchers, using elements well known in social networking. Such service shall make it easy to locate necessary databases and services on NEOs, broadcast observing plans, seek collaborators as well as offer free telescope time to others. NEODECS can potentially attract observers from other fields of astronomy, who have free resources but do not know that they can be used for NEO studies. While the information available at the beginning will be gathered by us (to reach a critical mass), the service will then live its own life and its content will be decided by the needs of its users.

Figure 1: A graph showing how various groups of users would interact with themselves using the NEODECS service.

NEODECS is developed under a contract to European Space Agency (ESA) and is thought of as an extension of the already existing ESA NEO portal (http://neo.ssa.esa.int) which is a central node for all European efforts in NEO studies. Comments on NEODECS received from the astronomical community indicate that it would be useful to open the service to other Small Solar System Bodies (SSSB). This should be easy since most of them share similar observing techniques.

3. Service architecture

NEODECS will offer two modes of use: for registered users, who will use it regularly, and for casual visitors, who will be given open access to most of the content. Registration will be possible after providing basic credentials, affiliation, type of research done (observations, modelling, etc.). Such data will allow our service to automatically create a link to the ADS and Astro-ph databases of publications, which will further characterize the activity of a given scientist.

Fig. 1 shows how researchers will interact with our service. For example, an observer who collects his re-

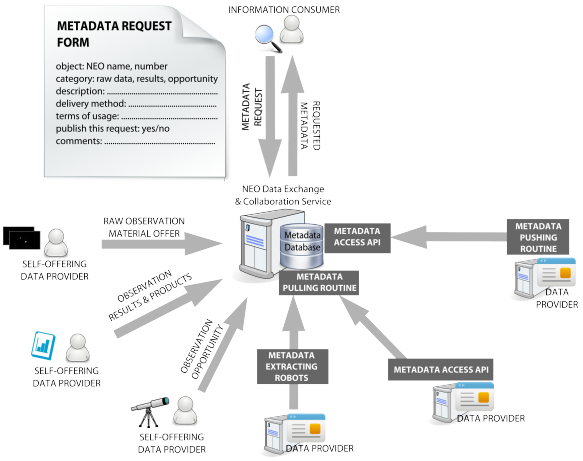

Figure 2: A structure of the NEODECS system

sults in a simple table on own webpage (”User having own data”), so that they are not dispersed in several papers, registers an URL to his data in NEODECS. Doing so he selects keywords (from a predefined list) describing parameters present in his table (like NEO rotation period, taxonomy, diameter, etc.). In case his data are still unpublished, he can register them providing a list of the observed objects and types of determined parameters, but instead of a URL pointing to the data he can request e-mail contact from those interested in using the data.

Such meta-data in NEODECS can then be searched by a ”Researcher using data”. As a result he will obtain a list of links to resources on the Internet (both published and unpublished). He can also register an ”Observation request” asking for data on object he is interested in. Such request should contain basic information on object’s visibility. If prolonged monitoring of the object is required, his request can be an invitation to join an observing campaign. In all such cases requests will be registered on the predefined web forms making it easy to enter most of the necessary information.

NEODECS shall also be useful to observers with free telescope time. They will be able to register an ”Observation offer” specifying the dates when their instruments would be available, conditions of collaboration (e.g. co-authorship of the paper), etc. A list of telescopes and instruments with a detailed description of their performance shall be created by observers upon registration so that offering them later would require only minimal interaction with the service.

Finally, NEODECS shall be connected to a general database on NEOs (like the NEODyS) which will be used for verification of some of the entered data (e.g. it will check if the object names are not misspelled).

A more technical presentation of the NEODECS structure is included in Fig. 2.

4. Related projects

Our consortium of Astronomical Observatory of A. Mickiewicz University and ITTI develops several NEO related web services under contracts to ESA. The NEO User Support Toolkit consists of several tools which should help NEO observers in preparation of their observation. It includes, among all, the planning tool (what and when to observe), and the sky chart tool (for producing finding charts), and is in the process of integration with the ESA NEO portal (`http://neo.ssa.esa.int`). Another service called SANORDA (Service for Archival NEO Orbital and Rotational Data Analysis) shall include, among all, web tools for determination of asteroid composite lightcurves and phase curves. It shall also contain an asteroid lightcurve database containing both the historical Asteroid Photometric Catalogue (the latest ”Helsinki version”) and a newer Asteroid Lightcurve Photometry Database (`http://alcdef.org/`). The former is based on the ATL format, and the later uses the ALCDEF format. It may be interested to readers that the APC catalogue, offered by the Helsinki Observatory together with a web service for data download, upload, and analysis, is no longer available. It has been archived and transferred to our Observatory so that we can use it for SANORDA. As the work on SANORDA shall start not earlier than in September 2017, we offer the archive version of the APC on the NEODECS webpage: `http://neodecs.eu`.

Acknowledgements

The NEODECS service is developed under the European Space Agency contract ESA-PLP 028.

EPSC Abstracts
Vol. 11, EPSC2017-865, 2017
European Planetary Science Congress 2017

Gaia space mission and asteroid spectroscopy

M. Delbo (1), L. Galluccio (1), F. De Angeli (2), F. Mignard (1), A. Cellino (3), P. Tanga (1)
(1) Université Côte d'Azur, Observatoire de la Côte d'Azur Lagrange, CNRS, France. (2) Institute of Astronomy. Cambridge, United Kingdom. (3) Istituto Nazionale di Astrofisica, Osservatorio Astronomico di Torino, Torino, Italy.
(delbo@oca.eu. / Fax: +33-4-92003028)

1. Introduction

The light of the Sun reflected by the surface of asteroids carries information about their *composition* [1, 2]. By dividing an astronomically observed asteroid spectrum by that of the Sun (or a solar analogue star) wavelength-by-wavelength, one derives the asteroid *reflectance spectrum (a.k.a. reflectivity)*, which is diagnostic of the composition (Fig. 1). In order to enhance compositional interpretation, *taxonomies* of asteroid spectra have been developed (Fig. 1).

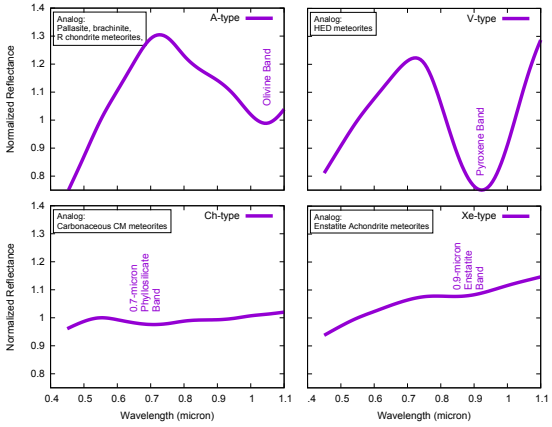

Figure 1: Average values of the reflectance spectra of A-, V-, Ch-, and Xe-types. Different types of reflectance spectra indicate different compositions. Adapted from ref.[2]

2. From BP/RP to asteroid reflectance

The visible-light spectra of asteroids is measured by Gaia using its Blue and Red photometers (BP and RP for short). (i) BP/RP epoch spectra are *internally* calibrated. (ii) Asteroids and solar analog stars are identified – amongst billions of stars – and their BP/RP calibrated epoch spectra are obtained from the Main Database of Gaia observations. (iii) Average BP/RP solar analog is obtained. (iv) Epoch reflectance spectra are obtained by dividing the BP/RP epoch spectra by the average solar analog. (v) The average reflectance spectrum is calculated for each asteroid.

3. Classification

The average reflectivities of all asteroids observed by Gaia will be classified using an unsupervised clustering algorithm [3]. Comparison of Gaia spectra with those of known asteroid spectral taxonomies [4, 1] are performed.

4. Preliminary Results

We are currently validating asteroid reflectance spectra obtained from Gaia BP/RP. Figure 3 shows some of the BP/RP reflectancies compared to ground based spectra. Although the Gaia asteroid spectra shown here are based on a preliminary *cycle 1 calibration*, the agreement is very good.

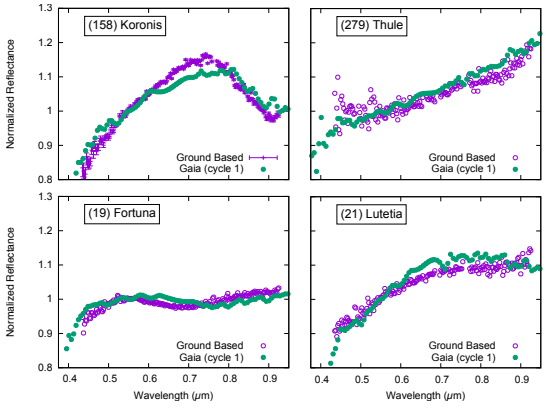

Figure 2: Gaia reflectance spectra of four asteroids with well known ground based spectra. The BP and RP data, which are calibrated independently, are merged in one single reflectance spectrum.

Acknowledgements

The Gaia asteroid spectra pipeline is run at the CNES in Toulouse, France.

References

[1] S J Bus, F Vilas, and M A Barucci. Visible-Wavelength Spectroscopy of Asteroids. *Asteroids III, W. F. Bottke Jr., A. Cellino, P. Paolicchi, and R. P. Binzel (eds), University of Arizona Press, Tucson.*, pages 169–182, 2002.

[2] F E DeMeo, C M O'D Alexander, K J Walsh, C R Chapman, and R P Binzel. The Compositional Structure of the Asteroid Belt. *Asteroids IV*, pages 13–41, 2015.

[3] L Galluccio, O Michel, P Bendjoya, and E Slezak. Unsupervised Clustering on Astrophysics Data: Asteroids Reflectance Spectra Surveys and Hyperspectral Images. In *CLASSIFICATION AND DISCOVERY IN LARGE ASTRONOMICAL SURVEYS: Proceedings of the International Conference: "Classification and Discovery in Large Astronomical Surveys". AIP Conference Proceedings*, pages 165–171. Hippolyte FIZEAU Laboratory, CNRS-University of Nice Sophia Antipolis; I3S Laboratoire, CNRS-University of Nice Sophia Antipolis 2000, route des Lucioles Les Algorithms-BP. 121-06903 Sophia Antipolis Cedex-France, AIP, December 2008.

[4] Francesca E DeMeo, Richard P Binzel, Stephen M Slivan, and Schelte J Bus. An extension of the Bus asteroid taxonomy into the near-infrared. 202(1):160–180, July 2009.

EPSC Abstracts
Vol. 11, EPSC2017-874, 2017
European Planetary Science Congress 2017

Photometry and model of a Very Small NEA 2015 AZ43

T. Kwiatkowski (1), D. Oszkiewicz (1), A. Kryszczyńska (1), P. Bartczak (1) , G. Dudziński (1) , K. Kamiński (1) , N. Moskowitz (2) , M. Willman (3), D. Polishook (4), A. Thirouin (2), W. Ryan (5), E. Ryan (5), A. Penttila (6), O. Vaduvescu (7), E. Unda-Sanzana (8), P. Pravec (9)

(1) Astronomical Observatory, Department of Physics, A. Mickiewicz University, Poznań, Poland (tkastr@vesta.astro.amu.edu.pl); (2) Lowell Observatory, Flagstaff, USA; (3) University of Hawaii, Pukalani, USA; (4) Department of Earth and Planetary Science, Weizmann Institute, Rehovot, Israel; (5) Magdalena Ridge Observatory of New Mexico Tech, Socorro, USA; (6) Department of Physics, University of Helsinki, Finland; (7) Instituto de Astrofisica de Canarias, La Laguna, Spain; (8) Unidad de Astronoma at Universidad de Antofagasta, Chile; (9) Astronomical Institute of the Academy of Sciences of the Czech Republic, Prague, Czech Republic

1. Introduction

Very Small Asteroids (VSAs) are objects with diameters $D < 150$ m. They often rotate with periods shorter than 2 h enabling us to study their internal structure by comparing the centrifugal force with the material forces holding them together. VSAs are sensitive to the YORP effect, which can change their spins and spin axes. For such reasons it is important to determine their shapes and spin axes. 2015 AZ43 is a Apollo asteroid with an effective diameter of about 60 m. From 6 to 23 Feb 2015 it swept a 120° long arc in the sky maintaining a decent brightness $V <$ 20 mag, spanning solar phase angles from 48 to 90, and staying away from the Milky Way. This prompted us to get its lightcurves at different geometries to use them for spin and shape modelling.

2. Observations

We observed 2015 AZ43 with 7 telescopes (2.5-m NOT at La Palma, 1.0-m and 2.0-m LCOGT, 4.0-m Mayall at Kitt Peak, 0.7-m RBT at Winer Obs. AZ, 2.4-m at MRO, and 1.5-m Danish Telescope at La Silla) during 13 nights obtaining 26 lightcurves. We also added a lightcurve observed independently by Brian Warner [1]. A rotation period from the Mayall lightcurve was also reported in [2]. An example lightcurve is presented in Fig. 1.

3. Model

Relatively high phase angles allowed us to use the SAGE algorithm [3] to derive a family of non-convex shapes of 2015 AZ43. We are currently analysing them to see if a unique solution can be derived. At this moment, for the purpose of illustration, we present

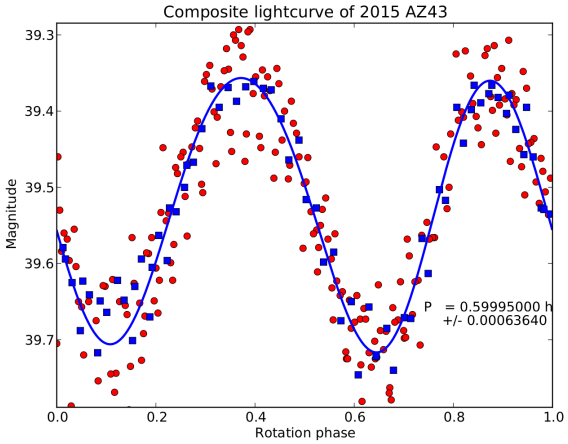

Figure 1: Example lightcurve obtained on Feb 11 simultaneously with the 0.7-m R. Baranowski Telescope in Arizona (red circles) and 1.0 LCOGT in Texas (blue squares). Zero phase JD=2457063.6246296.

a solution obtained with the sidereal period $P = 0.599868$ h and the spin axis $\lambda = 281°$, $\beta = -35°$ (Fig. 2).

Acknowledgments

The Mayall observations were done within the MANOS programme, supported by the NASA NEOO grant NNX14AN82G. The LCOGT observations were carried within the EURONEAR network.

References

[1] Warner, B (2015) MPB 42, 172

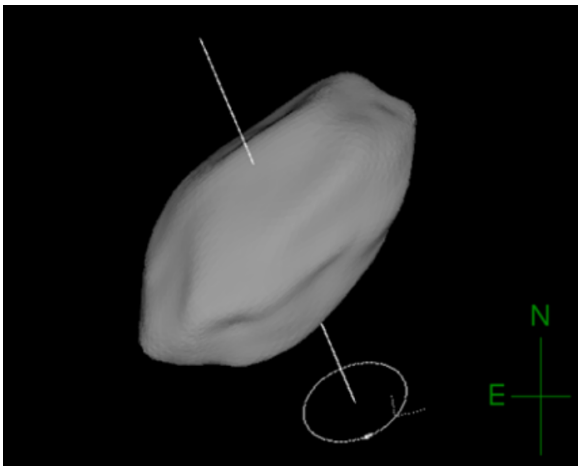

Figure 2: One of the solutions for a non-convex shape of 2015 AZ43. The model is viewed from an aspect angle of 132°.

[2] Thirouin, A et al. (2016) AJ 152, 163;

[3] [3] Bartczak et al. (2014) MNRAS 443, 1802;

EPSC Abstracts
Vol. 11, EPSC2017-902, 2017
European Planetary Science Congress 2017

New infrared telescopic observation of Vesta

E. Palomba (1,2), E. D'Aversa (1), T. Sato (3), A. Longobardo (1), S. Aoki (4), G. Sindoni (1), F. Oliva(1)
(1) INAF-IAPS, via Fosso del Cavaliere 100, 00133 Rome, Italy (ernesto.palomba@iaps.inaf.it); (2) ASI-ASDC, Rome, Italy; (3) ISAS-JAXA,Sagamihara City, Japan,; (4) Belgian Institute for Space Aeronomy, Bruxelles, Belgium

Abstract

In this work we present new telescopic observations of the Vesta asteroid made at the Subaru Telescope by using the COMICS IR spectrometer. We were able to obtain 5 different observations in 5 day, at two different epochs. The obtained spectra do not exhibit Reststrahlen bands and show only weak features attributable to the Christiansen peak and to the transparency feature compatible with a fine grain size regolith.

1. Introduction

Vesta have been explored and mapped in detail by the Dawn space mission [1]. The measurements obtained by the VIR spectrometer demonstrated that Vesta is the parent body of the HED meteorites [2], in which the pyroxene mineralogy varies locally. Small deposits of olivine were found in the northern hemisphere of the asteroid [3,4]. The regolith grain size has been suggested to be < 45 micron [5]. Nevertheless, plagioclases which are one of the most important mineralogical component of the HED have not been detected on the surface of Vesta yet, since they have not clear features in the NIR. In addition, due to orbital and geometrical constraints, the northern hemisphere was not mapped completely and in large part it is still not explored.

2. Observations and data reduction

Vesta was observed on 23-24 January 2016 with two consecutive observations of 30 minutes. The HD5112 was also observed as standard star, used for removing absorptions of Earth's atmosphere and estimating the seeing size. The air mass during the spectroscopic observations of Vesta was 1.205, whereas the exposure time was 0.904 s. Background (sky+telescope) was substracted from target spectra, then flat-field and spectral calibrations were performed. The successive data reduction operations were image transformation, shift-and-add spectra to improve SNR and retrieval of Vesta spectra by means of standard spectra.

3. Results

Comparison with previous telescopic observations

Vesta has been already observed in the mid-IR by the ISO telescope with ISO-PHOT instrument [6] and the Kuiper Airborne Observatory (KAO) [7]. After a preliminary re-analysis we discarded the KAO data because they are not reliable [Cohen, personal communication]. The ISO spectrum doesn't match at all with our new observations. By comparing the emissivities, the ISO spectrum exhibit a larger spectral contrast with a completely different behaviour from the Subaru ones. The Christiansen frequencies obtained with the Subaru and ISO are 8.52 and 9.08 μm, pointing to a pyroxene and olivine composition, respectively. We believe that both the very large spectral contrast and the composition retrieved by the ISO observation make these data a bit questionable

4. Conclusions

Our results are in line with what found by the Dawn space mission. The very low spectral contrast and the presence of a transparency feature indicate the presence of a very small grain size regolith, as suggested by some VIR analysis. The pyroxene composition is in agreement with the HED mineralogy. In addition preliminary analysis of the emissivity slopes could indicate, for the first time, the presence of plagioclases.

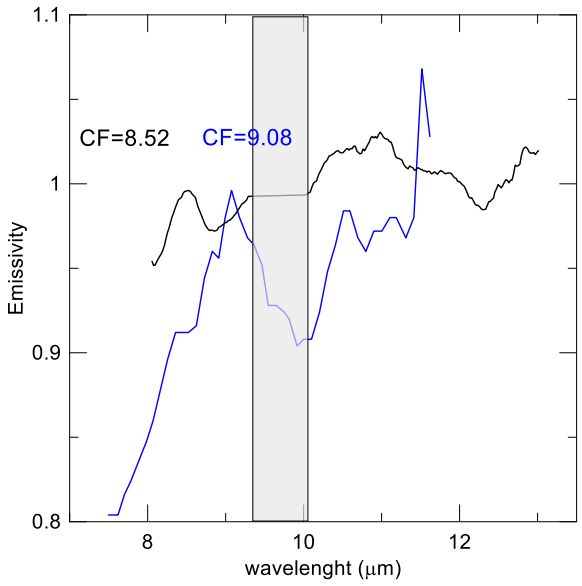

Figure 1. Vesta emissivity spectra. Subaru smoothed (black). ISO-PHOT (blue). The grey rectangle is a non-reliable spectral interval for the Subaru observation

References

[1] Russell, C.T., et al. (2011). Springer, ISBN: 978-1-4614-4902-7

[2] De Sanctis, M.C. et al. (2012), Science 336, 6082,697

[3] Ammannito, E. et al. (2013), Nature, 504, 122-125

[4] Palomba, E. et al. (2015), Icarus 258, 120-134

[5] Palomba, E. et al. (2014), Icarus 240, 58-72

[6] Dotto, E. et al. (2000), A&A 358, 2000/6/1 SP-133EP

[7] Cohen, M. et al. (1998), The Astronomical Journal 115, 4, 1671-1679

EPSC Abstracts
Vol. 11, EPSC2017-909, 2017
European Planetary Science Congress 2017

Analysis of homogeneity of the main belt asteroids families with the "color-albedo" plots

I. Slyusarev, D. Shymkiv
V.N. Karazin Kharkiv National University, Sumska str. 35, Kharkiv 61022, Ukraine, (i_slyusarev@mail.ru)

Abstract

Using color indexes from SDSS, WISE albedos for the 57 asteroids families from Nesvorny list we tested the homogeneity using the "color - albedo" plots. We found, that significant fraction of the analyzed families are inhomogeneous in terms of albedos and colours. A fraction of the dark subgroups is not negligible.

1. Introduction

A list of 122 asteroid families are given in [1], that includes more than 140000 asteroids. Asteroid families are easy to identify as clusters of orbits in the space of proper elements (a_p, i_p, e_p). They are interpreted as the observable outcomes of energetic collisional events, leading to complete disruption of original parent bodies. Family-forming collisions are expected to liberate material from a large fraction of the parent body's volume. A homogeneous parent body would produce a family with very narrow distributions of physical properties and a heterogeneous parent body would instead produce a family with wide or multimodal distributions. Analyzing data on physical properties of the family members we can also find possible interlopers in homogeneous families or we can distinguish overlapping of families in (a_p,i_p,e_p,) space. Here we test the physical homogeneity of asteroid families based on the color and albedo data.

2. Data

Main belt asteroid families were taken from [1], We have considered only numbered asteroids in our analysis. We use WISE albedos from [2] and a* which is the first principal component in the r-i versus g-r SDSS color-color plane [3,4] to plot albedo distributions and "albedo – color" diagram for each family.

3. Results

We have found that 15 asteroid families from 57 families included in our analysis demonstrated a bimodal albedo distribution. These results are well-seen on diagrams "albedo-color". As an example, Fig.1 and 2 show the plots for the Gefion family.

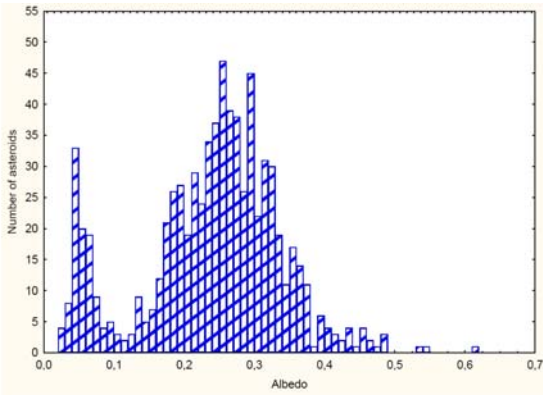

Figure 1: Albedo distribution for Gefion family.

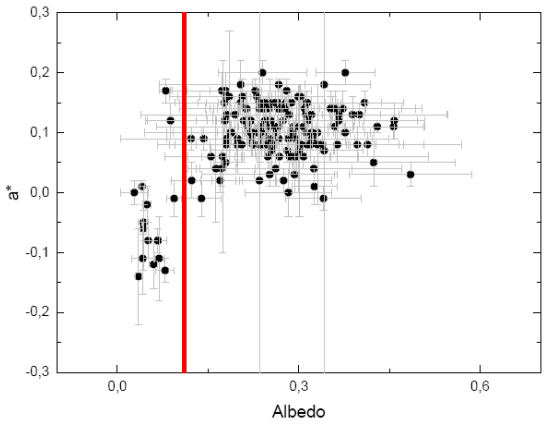

Figure 2: "Albedo – color" diagram for Gefion family.

For all bimodal families the dark subgroup has albedo smaller than 0.08÷0.11 (red line in Fig.2) and a*<0. Only two families (Vesta and Flora) with bimodal albedo distribution on the diagram "albedo-color" have shown, that they consist of three subgroups.

4. Conclusons

Significant amount (25%) of the analysed families are inhomogeneous in terms of albedos and colours. A fraction of the dark subgroups is not negligible (10-15%).

References

[1] Nesvorny, D., Nesvorny HCM Asteroid Families V3.0. EAR-A-VARGBDET-5-NESVORNYFAM-V3.0. NASA Planetary Data System, 2015;

[2] Mainzer, A.K., Bauer, J.M., Cutri, R.M., Grav, T., Kramer, E.A., Masiero, J.R., Nugent, C.R., Sonnett, S.M., Stevenson, R.A., and Wright, E.L., NEOWISE Diameters and Albedos V1.0. EAR-A-COMPIL-5-NEOWISEDIAM-V1.0. NASA Planetary Data System, 2016;

[3]http://www.astro.washington.edu/users/ivezic/sdssmoc/ADR4.dat;

[4] Parker et al.: The size distributions of asteroid families in the SDSS Moving Object Catalog 4, Icarus, Vol. 198, pp. 138–155.

EPSC Abstracts
Vol. 11, EPSC2017-924, 2017
European Planetary Science Congress 2017

Large asteroid families modelled by impact events

P. G. Benavidez (1,2), D. D. Durda (3), B. Enke(3), A. Campo Bagatin (1,2), D. C. Richardson (4), E. Asphaug (5) and W. F. Bottke (3)
(1) Departamento de Física, Ingeniería de Sistemas y Teoría de la Señal, (2) Instituto Universitario de Física Aplicada la Ciencias y la Tecnología, (3) Southwest Research Institute, (4) University of Maryland at College Park, (5) Arizona State University

Abstract

We present a study of large asteroid families modeled by impact events. To extend the work started by [1] and [2], we performed a new set of simulations in the gravity regime for monolithic and rubble-pile targets of 400 km diameter. Here we analyze and discuss if the studied families are best matched by the modeled size-frequency distribution (SFD) resulting from a monolithic or rubble-pile parent body.

1. Introduction

Many authors have used the fragment SFDs produced by impact simulations to glean insights into parent body sizes and disruption conditions for asteroid families (e.g., [1], [2], [3]. In particular, several authors have used the results of SPH codes to explore the disruption of $D > 100$ km-diameter parent bodies. Basically, what these studies do is plot to the same scale the modeled SFD and the observed family SFD in a single chart. Modeled impacts assume a particular target size; therefore, the resulting largest remnant and SFD of associated fragments may need to be offset to larger or smaller sizes to match the observed SFD. This offset suggests a larger or smaller parent body for the observed family. However, in some cases, especially when the parent body is actually quite different in size from the particular modeled target (usually 100 km diameter), the methodology used to date could provide results that are not entirely accurate. Specifically, the SFDs of $D >> 100$ km-diameter targets could have significantly different features compared to those for a $D = 100$ km target, i.e., relative mass of the largest fragment and/or the SFD slope of smaller fragments. This is because the effects of gravity in the reaccumulation process of such larger bodies do not simply scale linearly.

On this basis, we extend the systematic investigation of impact outcomes started by [1] and [2] to 400 km-diameter targets using the same range of impact conditions and two internal structures: monolithic and rubble-pile.

2. Modeled families' SFD

The procedure applied to determine families is detailed in [4]. We have considered asteroid families with an alternative estimation of the parent body size. That is, the progenitor size estimation is based on geometric considerations ([3] and [5]). Then, we selected families with large expected parent bodies (of order $D = 400$ km) to compare with our new set of simulations. This procedure ensures the shift is appropriately small, so we have higher confidence when matching the SFDs.

We investigated four asteroid families: Hygiea, Vesta, Themis and Eunomia. To measure a match between our simulation and the observed families we calculate the chi-square statistic (χ^2) to find the best matches for both monolithic and rubble-pile targets.

3. Results and Conclusions

For the Hygiea family, a good match was found that corresponds to a cratering event onto a rubble-pile target involving a projectile of $D = 54.4$ km at 7 km/s and impact angle of 60°. Regarding the monolithic target, all the "best" potential cases have problems fitting the size range from ~25 to ~70 km-diameter. Then, the parent body of the Hygiea family could have a rubble-pile internal structure of 416 km diameter.

For the Eunomia and Vesta families we found fairly good matches. For Eunomia, the best match corresponds to a super-catastrophic breakup onto a monolithic target that was impacted by a projectile of D ~186 km at 6 km/s and impact angle of 45°. The results suggest that the parent body of the Eunomia family could be a monolithic body of 382 km diameter. Regarding impact simulations with a rubble-pile target, we found at least four different

impact conditions that match the observed SFD for fragments larger than D ~25 km. However, below this size, the modeled SFD slope became shallower than the observed one. We rule out these cases on this basis. On the other hand, [6] found two subfamilies within Eunomia, which they attribute to separate cratering events. This could suggest that some collisional process happened in this family, modifying its SFD at some level. Then, this could explain why the matches found are fairly acceptable but not perfect. It should be studied carefully in future work.

For the Vesta family, an impact simulation with a monolithic target impacted by a projectile of D ~100 km at 6 km/s and impact angle of 75° is the one that best matches the observed SFD. The agreement is quite good for fragments of D > 15 km, but below this size the modeled SFD slope remains very steep, as is usual for such oblique impacts. The parent body size estimated from this impact is D = 468 km, in good agreement with the geometrical estimation.

For the Themis family, it was not possible to find a good match. From either monolithic or rubble-pile targets it is possible to match the largest fragment and the SFD slope for D < 60 km, however it is hard to reproduce the observed bump around D = 100 km. The χ^2 value suggests that the SFDs of rubble-pile cases are closer to the observed one, but there are no really satisfactory matches because the bump is not as bulging as in the Themis SFD. The fact we could not find an acceptable match for this family could be due to several reasons:

a) The modeled internal structures in this work are very simple and the Themis family could have a more complex internal structure.
b) The existence of the Beagle subfamily indicates that the Themis family has undergone some collisional activity over time.
c) It could be possible that the Themis parent body had a size $D \sim 250 - 300$ km or different bulk density than the simulated targets.

We suggest that an extension of impact simulation models to differentiated targets is necessary to build a more complete picture of the impact physics. It would helps to constrain the impact conditions of the Themis family and likely other families.

Acknowledgements

This work was partly supported by the Spanish Ministerio de Ciencia e Innovacion (now expired) grant AYA2011-30106-C02-02.

References

[1] Durda, D. D. et al. Size-frequency distributions of fragments from SPH/*N*-body simulations of asteroid impacts: Comparison with observed asteroid families. Icarus 186, 498–516, 2007.

[2] Benavidez, P. G. et al. A comparison between rubble-pile and monolithic targets in impact simulations: Application to asteroid satellites and family size distributions. Icarus 219, 57. 2012.

[3] Tanga, P., Cellino, A., Michel, P., Zappalà, V., Paolicchi, P., & dell'Oro, A. On the size distribution of asteroid families: The Role of Geometry. Icarus 141, 65–78, 1999.

[4] Nesvorný, D., Jedicke, R., Whiteley, R. J., & Ivezić, Ž. Evidence for asteroid space weathering from the Sloan Digital Sky Survey. Icarus 173, 132–152, 2005.

[5] Campo Bagatin, A., & Petit, J.-M. Effects of the geometric constraints on the size distributions of debris in asteroidal fragmentation. Icarus 149, 210, 2001.

[6] Milani, A., Cellino, A., Knežević, Z., Novaković, B., Spoto, F. & Paolicchi, P. Asteroid families classification: Exploiting very large datasets. Icarus 239, 46, 2014.

EPSC Abstracts
Vol. 11, EPSC2017-941, 2017
European Planetary Science Congress 2017

UV Spectroscopy of Metallic Asteroid (16) Psyche

N. J. Cunningham (1), T. M. Becker (2), K. D. Retherford (2), L. Roth (3), L. M. Feaga (4), J.-E. Wahlund (5) and L. T. Elkins-Tanton (6)
(1) Nebraska Wesleyan University, USA (ncunning@nebrwesleyan.edu), (2) Southwest Research Institute, Texas, USA, (3) Royal Institute of Technology, Stockholm, Sweden, (4) University of Maryland, USA, (5) Swedish Institute of Space Physics, Kiruna, Sweden, (6) Arizona State University, USA

Abstract

Asteroid (16) Psyche is the largest M-type asteroid, and the planned destination of the NASA Discovery mission Psyche [1] and the proposed ESA M5 mission Heavy Metal. Psyche is considered to be the exposed core of a differentiated asteroid, whose mantle has been stripped by collisions [2]; but other histories have been proposed. We observed Psyche with the Space Telescope Imaging Spectrograph (STIS) and Cosmic Origins Spectrograph (COS) aboard the Hubble Space Telescope, to obtain a full ultraviolet (UV) spectrum of both of Psyche's hemispheres. We seek to test three possible scenarios for Psyche's origin: Is Psyche the exposed core of a differentiated asteroid? Is it an asteroid with high olivine content that has been space-weathered? Or did Psyche accrete as-is in a highly-reducing environment early in the history of the solar system? We will present the UV spectra and their implications for Psyche's history.

1. Introduction

Like other M-type asteroids in the Tholen classification scheme [3], Psyche exhibits a relatively featureless, red-sloped spectrum in the visible and near-IR. Its high radar albedo [4], high density [5], and high thermal inertia [6] support the leading theory, that Psyche represents a dense, exposed metal core. An alternate proposal suggests that rather than being developed through collisional stripping, Psyche accreted from highly-reduced, metal rich material near the Sun early in the formation of the solar system [1]. A third possibility is that Psyche (and some other M-type asteroids) may have formed as differentiated bodies with metal cores; but their olivine-rich mantles, rather than being collisionally stripped, were processed by space weathering so that the 1 μm olivine absorption feature is weakened and spectrally shifted to shorter wavelengths [7]. Psyche and some other M-type asteroids show a weak absorption band near 0.9 μm.

Laboratory studies [8] find that the UV spectral region is more sensitive to different mineral properties than longer wavelengths, motivating our study.

2. UV Spectral Indicators

Specific features targeted by our study include: Fe3+–O and Fe2+–O absorption bands at 210–230 nm and 250–270 nm, respectively, shown to be intense and identifiable in lab spectra within many minerals common to planetary surfaces [8]; and "blueing" of spectral slope at short UV wavelengths. The presence of Fe–O bands in the absence of spectral blueing, for example, would give support to the theory of Psyche as a more recently-exposed metallic core. Conversely, the lack of Fe–O absorption features together with spectral evidence of space weathering would lend credence to the formation in a reducing environment closer to the Sun.

3. Preliminary Spectra

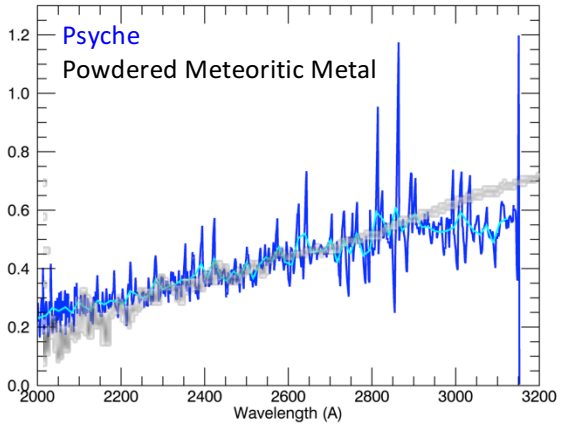

Figure 1: STIS spectrum of one hemisphere of Psyche (raw spectrum divided by solar spectrum); vertical axis is arbitrarily scaled. Graphed laboratory spectrum from [8] overlaid for comparison.

STIS spectra of both hemispheres, shown in figures 1 and 2, are similar, and exhibit a slope similar to that found in laboratory measurements of non-oxidized powdered meteoric metals [8].

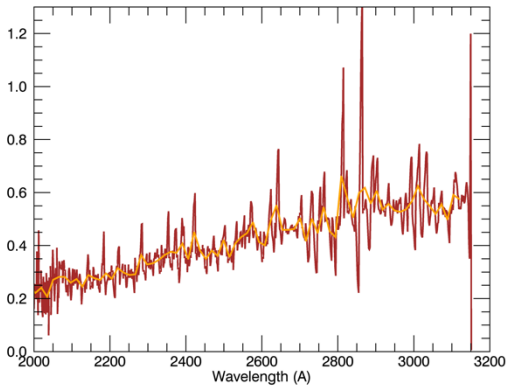

Figure 2: Preliminary STIS spectrum of Psyche, after dividing by solar spectrum; opposite hemisphere from Figure 1.

The slopes of laboratory-measured orthopyroxenes [8] are shallower than the slope observed in our spectra.

4. Summary and Conclusions

Full analysis of our UV spectra of Psyche are underway. Preliminary spectra appear to indicate large-scale homogeneity in Psyche's surface, with similar spectra for both observed hemispheres. We note no clear Fe–O band absorption features, and find a UV spectral slope similar to the laboratory measurements of meteoric metal powder. The lack of Fe-O bands is surprising for an iron body that has been exposed to space weathering, and could indicate (1) that the surface of Psyche has not long been exposed to space weathering (and is therefore young); (2) more work is needed to understand how space weathering affects M-type asteroids; or perhaps (3) the surface is protected from weathering by a magnetic field.

Acknowledgements

This work is based on observations made with the NASA/ESA Hubble Space Telescope, obtained through the Space Telescope Science Institute, which is operated by the Association of Universities for Research in Astronomy, Inc., under NASA contract NAS 5-26555. These observations are associated with program number HST-GO-14609.

References

[1] Elkins-Tanton, L.T. et al.: Asteroid (16) Psyche: the science of visiting a metal world, 47th Lunar & Planetary Science Conference, 1631, 21-25 March 2016, The Woodlands, Texas, USA, 2016.

[2] Asphaug, E., Agnor, C. B., and Williams, Q.: Hit-and-run planetary collisions, Nature, Vol. 439, pp. 155-160, 2006.

[3] Tholen, D.J.: Asteroid taxonomy from cluser analysis of photometry, thesis, Univ. of Arizona, Tucson, USA, 1984.

[4] Ostro, S. J., Campbell, D. B. and Shapiro, I. I.: Mainbelt asteroids: dual-polarization radar observations, Science, Vol. 229, pp. 442-446, 1985.

[5] Kuzmanoski, M. and Kovačević, A.: Motion of the asteroid (13206) 1997GC22 and the mass of (16) Psyche, Astronomy & Astrophysics, Vol. 395, pp. L17 -L19, 2002.

[6] Matter, A., Delbo, M., Carry, B., and Ligori, S.: Evidence of a metal-rich surface for the Astroid (16) Psyche from interferometric observations in the thermal infrared, Icarus, Vol. 226, pp. 419-427, 2013.

[7] Britt, D., Kohout, T., Schelling, P., and Consalmagno, G. J.: Space weathering in olivine and the mineralogy of (some) M-class asteroids, Division for Planetary Science Meeting #46, 506.01, 9-14 November 2014, Tucson, Arizona, USA, 2014.

[8] Cloutis, E.A. et al.: Ultraviolet spectral reflectance properties of common planetary minerals Icarus, Vol. 197, pp. 321- 347, 2008.

EPSC Abstracts
Vol. 11, EPSC2017-952-1, 2017
European Planetary Science Congress 2017

The global topography of Bennu: altimetry, photoclinometry, and processing

M. E. Perry[1], O. S. Barnouin[1], M. G. Daly[2], J. Seabrook[2], E. E. Palmer[3], R. W. Gaskell[3], K. L. Craft[1], J. H. Roberts[1], L. Philpott[4], M. Al Asad[4], C. L. Johnson[3,4], A. H. Nair[1], R. C. Espiritu[1], M. C. Nolan[5], and D. S. Lauretta[5], [1]Johns Hopkins Applied Physics Laboratory, Laurel MD, USA (mark.perry@jhuapl.edu), [2]York University, Toronto, M3J 1P3, [3]Planetary Science Institute, Tucson, AZ 85719, [4]Univ. of British Columbia, Vancouver, V6T 1Z4, [5]Univ. of Arizona, Tucson, AZ.

1. OSIRIS-REx

The Origins, Spectral Interpretation, Resource Identification, and Security–Regolith Explorer (OSIRIS-REx) mission will spend two years observing (101955) Bennu and will then return pristine samples of carbonaceous material from the asteroid [1]. Launched in September 2016, OSIRIS-REx arrives at Bennu in August 2018, acquires a sample in July 2020, and returns the sample to Earth in September 2023. The instruments onboard OSIRIS-REx will measure the physical and chemical properties of this B-class asteroid, a subclass within the larger group of C-complex asteroids that might be organic-rich. At approximately 500m in average diameter [2], Bennu is sufficiently large to retain substantial regolith and as an Apollo asteroid with a low inclination (6°), it is one of the most accessible primitive near-Earth asteroid.

2. The AltWG

The Altimetry Working Group (AltWG) produces local and global topographic maps (digital terrain maps or DTMs) for science objectives [2] and for navigation, including Natural Feature Tracking (NFT) [3] used to autonomously guide OSIRIS-REx to the sample location on Bennu's surface. The AltWG generates the DTMs using two independent processes and datasets: stereo-photoclinometry (SPC) processing [4, 5] of images and analysis of range data obtained by the OSIRIS-REx Laser Altimeter (OLA [6]). The AltWG produces detailed data on the craters, surface topography, and data essential for interior-structure modeling. The DTMs are essential for characterizing the candidate sample sites, assessing their viability and value for sampling, and providing high-resolution feature for NFT. With each global DTM, the AltWG produces a suite of ancillary data that include gravitational potential, slope, and tilt maps. Combining OLA data with the SPC products generates the final, highest-fidelity version of these products [7]. The AltWG created a high-resolution (5cm) "truth" shape model of Bennu to develop and test processing and analysis tools.

3. OLA instrument

OLA is a dual-transmitter, high-rate scanning laser altimeter, built by MDA, and contributed by the Canadian Space Agency. During the Orbit-B phase of the mission, OLA will obtain global coverage in 6°x6° scans acquired every 2.5 minutes using the low-energy laser. Each scan covers a 80x80m section of the surface with 1.3×10^6 measurements with 7-cm spacing and spot size. During the Reconnaissance Phase, the spot size and spacing decrease to 2.5 cm.

Table 1: OLA performance and key characteristics for both the high- and low-energy modes.

Specification	High Energy	Low Energy
Maximum Operational Range	9.0 km	1.2 km
Minimum Operational Range	0.26 km	0.036 km
Range Accuracy (1σ)	< 0.31 m	< 0.06 m
Range Precision (1σ)	< 0.026 m	< 0.011 m
Scanner Field of Regard	$\pm 10^o$, $\pm 6^o$	$\pm 10^o$, $\pm 6^o$
Scanner Precision	< 20μrad	< 20μrad
Laser Divergence (1/e)	200μrad	100μrad
False Alarms	$< 10^{-6}$	$< 10^{-6}$
Probability of Detection	> 99.99%	> 99.99%
Clear Aperture	75 mm	75 mm
Pulse Energy	0.7 mJ	10 μJ
Pulse Duration	5 ns	1ns

4. OLA processing

Using the truth model of Bennu, we constructed an OLA test dataset that included statistical variations in range, trajectory, and pointing that were consistent with anticipated uncertainty in the reconstructed parameters. The simulations included the effects of laser beam divergence. The result is a set of 340 to 370 overlapping, ~80m x 80m raster scans or 3-D point clouds of the asteroid surface, each containing approximately 1.3 million laser range returns.

A keypoint-matching method reduces the data processing by registering hundreds of keypoints rather than the entire point cloud. Keypoints are features with distinctive characteristics that can be located and registered between scans. First, the ranges in each scan are converted to a 10-cm grid using the Generic Mapping Tools (GMT [8]). The 2-D Laplacian of these surfaces is then calculated to remove the curvature. VLFeat tools [9] locate

keypoints and calculate keypoint descriptors, which are 128-bit representations of the local surface gradients. A VLFeat algorithm finds the matching keypoints between each pair of overlapping scans, and initial global registration is performed by sequentially registering each scan to the overlapping keypoints of the previous scans using an Iterative Closest Point (ICP) algorithm. All registration is by rigid rotation and translation.

During the sequential registration, alignment errors accumulate and propagate. An iterative Generalized Procrustes Analysis (GPA [10]) is used to globally distribute registration errors. The last step is to apply the final transform of the keypoints of each scan to all the ranges in each point cloud and to construct a gridded global shape model. Fig. 1 shows the result of one test of the process. Later, high-resolution OLA scans, with 2-3 cm ground sample distance (GSD), are individually registered to the global shape model.

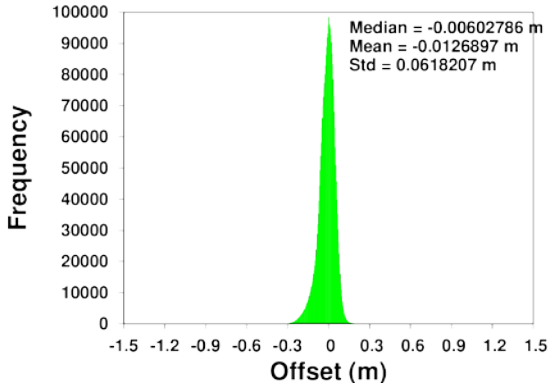

Figure 1: Difference histogram between the truth model and a DTM constructed from simulated OLA data. The requirement is 14-cm accuracy.

5. SPC processing

By analysing the brightness of pixels illuminated at different angles, the SPC process constructs slope and topography maps of the surface. The intermediate products are a set of landmark maps that can be used to build DTMs that match the best resolution of the source images. SPC has been used to produce accurate DTMs of Eros, Phobos, Mimas, Lutetia, Itokawa, Vesta, comet 67P, Mercury, and the Moon [c.f., 4, 5, 11]. To assess SPC performance at Bennu, we used the baseline observing plan to independently simulate 7,000 images of Bennu from the truth model, and then used SPC to generate a shape model using those images. The simulated images included trajectory and pointing errors. SPC will produce a 75-cm global model two weeks after the Preliminary Survey phase, and a 35-cm global model after the Detailed Survey phase. These DTMs will support optical navigation around Bennu.

SPC processing requires a range of incidence and emission angles, and the baseline mission [1] provides a data set that is sufficient for SPC to generate the required models. The height root mean squared (RMS) value between the truth and model shapes bettered the mission requirement of 75cm with a 51-cm RMS. For global models with 18-cm GSD, the RMS was 10cm. SPC will also produce local DTMs with smaller GSD. Fig. 2 shows a cross section of the truth and model over the sample site, and illustrates the excellent performance of the SPC-model. For smaller DTMs with GSD <35cm, we also use a cross-correlation technique to evaluate topography, the same technique to be used by the spacecraft to navigate to the sample site.

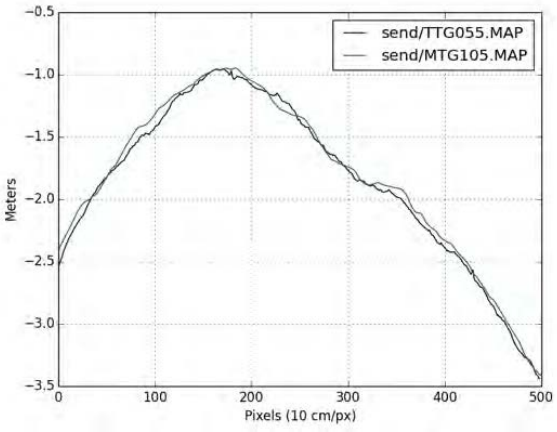

Figure 2: Cross-section of sample site showing model (green) and truth (black). The GSD is 10cm.

References

[1] Lauretta, D. S., et al. (2017) Space Sci. Rev. in press. [2] Beshore E. et al. (2015) *IEEE Aerospace Conf.* [3] Lorenz D. A. (2017) *IEEE Aerospace Conf.* [4] Gaskell R.W. et al. (2008) *Meteoritics & Planet. Sci., 43*, 1049-1061. [5] Gaskell R.W. et al. (2012) DPS, #209.03. [6] Daly M. G. et al. (2017) Space Sci. Rev. in press. [7] Roberts J. H. et al. (2017) *LPS XLVIII*. [8] Wessel P. et al. (2013) *EOS Trans. AGU, 94*, 409-410. [9] Vedaldi A. and Fulkerson B. (2010) *MM '10. ACM*, 1496-1472. [10] Toldo R. et al. (2010) *3DPVT 2010 Conference* [11] Palmer E.E. (2016) EPSL 3

EPSC Abstracts
Vol. 11, EPSC2017-957, 2017
European Planetary Science Congress 2017

Optimizing initial asteroid orbit determination of Gaia with normal point calculation

G. Fedorets (1,2, grigori.fedorets@helsinki.fi), K. Muinonen (1), T. Pauwels (3), M. Granvik (1) & P. Tanga (4) on behalf of the Gaia Solar system object team. (1) University of Helsinki, Finland (2) Nordic Optical Telescope, La Palma, Spain (3) Royal Observatory of Belgium (4) Observatoire de la Côte d'Azur, Nice, France.

Part of the work of the Data Processing and Analysis Consortium (DPAC) of ESA's Gaia mission involves producing accurate astrometry of known asteroids as well as discovery of new asteroids in the Solar system (Mignard et al. 2007, Tanga et al. 2016).

A basic unit of Gaia asteroid observations is called a transit, which comprises several positions of a moving target during the passage of the appropriate part of the sky by Gaia. Each transit comprises 4-10 observations. Transits are then bundled together to comprise a set of observations. From these observations, a swarm of possible orbits is calculated by an orbital inversion method called random-walk statistical ranging (Muinonen et al. 2016). The short-term processing of asteroid observations is dedicated to unknown objects. Orbits unmatched with known asteroids are then propagated for follow-up observations by ground-based observatories.

With the evolving of the short-term processing of the astrometry of Gaia, there has been an understanding that there is room for improvement in orbit calculation. A deeper understanding and use of various engineering data of the Gaia spacecraft (different attitudes) has yielded the necessity to split the observational errors into a systematic and random part. Previously, each point within the transit was treated as an independent observation. With the introduction of separate error sources this is no longer the case, since the systematic part of the error is common to all points within the transit. The uncertainties caused by the fluctuations of Gaia's attitude are a dominant factor in the systematic error. The fact that the time scale of fluctuations are of the same order as the duration of the transit make the systematic error a dominant factor.

Simple addition of systematic and random errors into combined covariance matrices may lead to near-singular matrices. We therefore propose an approach of collapsing all the points within a transit into a single normal point, calculated by the linear least-squares method at the mid-epoch of each transit. The random error of a normal point, calculated as the mean of all random errors within the transit, is then added with the systematic error for the entire transit. As a result, we expect to decrease the prediction area for follow-up observations for the majority of targets.

Gaia asteroid observations are comprised of several consequent short single observational arcs with varying systematic errors between each arc. The proposed method is particularly suitable for such cases. We anticipate that this method may be found helpful also for other asteroid surveys with cadences and error variabilities similar to Gaia.

References

[1] Mignard, F., Cellino, A., Muinonen, K., Tanga, P., Delbò, M., Dell'Oro, A., Granvik, M., Hestroffer, D., Mouret, S., Thuillot, W. & Virtanen, J. (2007). The Gaia mission: expected applications to asteroid science. *Earth, Moon, Planets* **101 (3-4)**, 97–125.

[2] Tanga, P., Mignard, F., Dell'Oro, A., Muinonen, K., Pauwels, T., Thuillot, W., Berthier, J., Cellino, A., Hestroffer, D., Petit, J.-M., Carry, B., David, P., Delbó, M., Fedorets, G., Galluccio, L., Granvik, M., Ordenovic, C. & Pentikäinen, H. (2016). The daily processing of asteroid observations by Gaia. *Planetary and Space Science* **123** 87 – 94.

[3] Muinonen, K., Fedorets, G., Pentikäinen, H., Pieniluoma, T., Oszkiewicz, D., Granvik, M., Virtanen, J., Tanga, P., Mignard, F., Berthier, J., Dell'Oro, A., Carry, B. & Thuillot, W. (2016). Asteroid orbits with Gaia astrometry using random-walk statistical ranging. *Planetary and Space Science* **123** 95 – 100.